ORNL/TM-2021/2330

Impacts of LEU+ and ATF on Fresh Fuel Storage Criticality Safety

A. M. Shaw
J. B. Clarity

February 2022

OAK RIDGE National Laboratory

ORNL IS MANAGED BY UT-BATTELLE LLC FOR THE US DEPARTMENT OF ENERGY

ORNL/TM-2021/2330

Nuclear Energy and Fuel Cycle Division

IMPACTS OF LEU+ AND ATF ON FRESH FUEL STORAGE CRITICALITY SAFETY

A. M. Shaw
J. B. Clarity

February 2022

Prepared by
OAK RIDGE NATIONAL LABORATORY
Oak Ridge, TN 37831-6283
managed by
UT-BATTELLE LLC
for the
US DEPARTMENT OF ENERGY
under contract DE-AC05-00OR22725

CONTENTS

LIST OF FIGURES

LIST OF TABLES

ABSTRACT

The use of increased fuel enrichment, which is still in the realm of low-enriched uranium (LEU) fuel, has been of interest to commercial light water reactor operators as part of the next iteration in fuel cycle technological advances and research and development. Using increased enrichment fuel, or high-assay LEU (HALEU), in power plants has clear benefits for being able to load cores with additional power-producing fuel. Although HALEU enrichments can range up to 20%, the more guarded approach of investigating enrichments above current fuels within 10% enrichment is referred to as *LEU plus (LEU+)* to reflect the less drastic change in operating conditions and requirements and similarity to current fuel cycles. Of additional interest and increasing maturity is the incorporation of accident-tolerant fuel (ATF) concepts, which are also applicable to the current fleet. This class of technologies involves changes such as cladding (e.g., chromium coating or FeCrAl) and fuel composition (e.g., chromia dopant) alterations to demonstrate improved fuel performance under accident scenarios. The ability to properly store fuel before and after residence time in the reactor is crucial to plant operation. Typically, this is done in either a new fuel vault (NFV) or spent fuel pool (SFP). Storing, loading, and unloading dozens of fuel assemblies within the same general area provides opportunities for obvious criticality concerns. These concerns are addressed with regulations to the subcriticality margin that the NFV and SFP must maintain in certain conditions. Adopting LEU+ fuel results in inherent reactivity increases, which are extremely relevant for safe fuel storage. Therefore, a clear understanding of the effects of LEU+ fuel and ATF on criticality safety margins to regulatory limits is required, as well as an understanding of the degree of absorber crediting under normal and accident conditions.

1. INTRODUCTION

The fuel changes needed to support proposed fuel cycle enhancements will greatly affect safety analyses performed to support the enrichment, fabrication, transportation, irradiation, and storage of nuclear material. This report investigates the impact of fuel design changes on the storage of unirradiated fuel once it is delivered to the reactor sites.

When fuel is brought onsite, it is typically unloaded from the shipping packages and placed in the new fuel vault (NFV) for inspection and then brought into the fresh fuel storage area of the spent fuel pool (SFP) before being loaded into the core. The racks in the NFV, SFP, and fuel-handling procedures throughout the plant are currently designed with a maximum fuel enrichment of 5.0 wt %. If utilities elect to increase the enrichment or change the form of the fuel to be more accident tolerant , how these changes affect the criticality safety analyses must be evaluated. This work used analyses for NFVs and SFPs obtained from publicly available source documents to develop baseline models of fresh fuel storage configurations, which are indicative of current criticality safety analyses. Based on these configurations, sensitivity calculations are performed to investigate the reactivity impacts of low-enriched uranium (LEU) plus (LEU+) and accident-tolerant fuel (ATF) fuel types. For cases in which the sensitivity calculations show that LEU+ fuel would result in higher than acceptable configuration reactivities, credit for mitigating features such as integral burnable absorbers is applied.

Section 2 describes the codes, methods, and models used in this analysis. Section 3 presents the results of the selected vault modeling with LEU+ and ATF implementations, details the effect of crediting integral burnable absorbers to offset LEU+ reactivity increases, and addresses modeling considerations which could be accounted for in a licensing application to determine the effect of enrichment on effects such as neutronic decoupling or the conservatism in averaging boiling water reactor (BWR) radial enrichments.

2. CODES, REGULATIONS, AND MODELS

2.1 CRITICALITY SAFETY ANALYSIS SEQUENCES/KENO V.A

The Criticality Safety Analysis Sequences with KENO V.a (CSAS5) provides a reliable, efficient means of performing k_{eff} calculations for systems routinely encountered in engineering practice. The CSAS sequences implement XSProc to process material input and provide a temperature and resonance-corrected cross section library based on the physical characteristics of the problem being analyzed [1].

The KENO V.a Monte Carlo code uses a simplified geometry package that allows for computational efficiency and was specifically designed to model light water reactor (LWR) fuel geometries for licensing evaluation calculations [1]. Because of the standard lattice geometries involved with commercial BWR and pressurized water reactor (PWR) operation and storage, KENO V.a is sufficient for describing the vaults and storage pools in this work. KENO V.a supports continuous energy and multigroup cross sections with multiple nuclear data libraries and group structures. For this work, the CSAS5 sequence uses the KENO V.a transport solver to search for the best estimate criticality eigenvalue (k_{eff}). All but several specific and noted models used the ENDF/B-VII.1 252-neutron group cross sections with square pitched lattice cell data to account for effects of resonance self-shielding. The cross section processing was performed by using CENTRM, which generated the problem-dependent libraries. SCALE 6.2.4 was used for all calculations. A study was performed that compared the results of the continuous energy and multigroup k_{eff} values as a function of moderator density in Section 3.1.2. The uncertainty in each calculation is 0.00010 Δk_{eff}, resulting in an uncertainty on each deviation between two points of 0.00014 Δk_{eff}.

2.2 APPLICABLE REGULATIONS

A review of the applicable regulations allows for understanding of the various analytical techniques used for the NFV and SFP configurations analyzed. The regulations that govern storage and handling of fuel at reactors are provided in 10 CFR 50.68, *Criticality Accident Requirements* [2], which states the following:

(1) Plant procedures shall prohibit the handling and storage at any one time of more fuel assemblies than have been determined to be safely subcritical under the most adverse moderation conditions feasible by unborated water.

(2) The estimated ratio of neutron production to neutron absorption and leakage (k_{eff}) of the fresh fuel in the fresh fuel storage racks shall be calculated assuming the racks are loaded with fuel of the maximum fuel assembly reactivity and flooded with unborated water and must not exceed 0.95, at a 95 percent probability, 95 percent confidence level. This evaluation need not be performed if administrative controls and/or design features prevent such flooding or if fresh fuel storage racks are not used.

(3) If optimum moderation of fresh fuel in the fresh fuel storage racks occurs when the racks are assumed to be loaded with fuel of the maximum fuel assembly reactivity and filled with low-density hydrogenous fluid, the k_{eff} corresponding to this optimum moderation must not exceed 0.98, at a 95 percent probability, 95 percent confidence level. This evaluation need not be performed if administrative controls and/or design features prevent such moderation or if fresh fuel storage racks are not used.

(4) If no credit for soluble boron is taken, the k_{eff} of the spent fuel storage racks loaded with fuel of the maximum fuel assembly reactivity must not exceed 0.95, at a 95 percent probability, 95 percent confidence level, if flooded with unborated water. If credit is taken for soluble

boron, the k_{eff} of the spent fuel storage racks loaded with fuel of the maximum fuel assembly reactivity must not exceed 0.95, at a 95 percent probability, 95 percent confidence level, if flooded with borated water, and the k_{eff} must remain below 1.0 (subcritical), at a 95 percent probability, 95 percent confidence level, if flooded with unborated water.

The following section discusses how these regulations are complied with in NFV and SFP analyses.

2.3 NEW FUEL VAULT ANALYSIS

The NFV racks are designed to allow for fuel that has recently been unloaded from shipping packages to be inspected before being loaded into the SFP. The NFV rack structures are dry under normal conditions with the racks typically consisting of metal angle irons or another open structure capable of supporting the fuel. It is common for NFV racks to be in a recessed area surrounded by concrete. Typically, modeling the neutron reflection of the concrete is important to the criticality safety calculations. The 10 CFR 50.68 (2) regulation dictates that the k_{eff} of the NFV be shown to be less than 0.95 at a 95% probability and 95% confidence level when fully flooded with unborated water. The 10 CFR 50.68 (3) regulation dictates that the k_{eff} of the NFV be shown to be less than 0.98 when filled with a low-density hydrogenous substance. In practice, the regulations are satisfied by performing analyses at a range of moderator densities varying between fully flooded and dry. The results of the 1.0 g/cm^3 are compared with the 0.95 limit, and the results of the calculations for all densities below 1.0 g/cm^3 are compared with the 0.98 limit. Conditions are not analyzed in cases in which a moderation condition is not credible because of mitigating circumstances in the plant.

The first step was to discover and develop representative NFV analyses for a PWR and BWR configuration. These were found by using the US Nuclear Regulatory Commission's Agencywide Documents Access and Management System (ADAMS) public database with baseline KENO-V.a models developed based on the vault descriptions provided in the final safety analysis report (FSAR) analyses. The configurations were analyzed with their baseline enrichments of 4.7 wt % for the BWR case and 5.0 wt % for the PWR case. Both cases were then analyzed with increased enrichments of 6.5 and 8 wt %. The PWR NFV analyses were performed for a full range of moderator densities. The BWR NFV analyses were performed for a density of only 1.0 g/cm^3 because a review of practices in other works [3–8] indicated that it is typical to mitigate the possibility of the optimum moderation condition. In addition to the best estimate k_{eff} values calculated for each of these models, the reactivity biases and uncertainties due to the uncertainties in material dimensions and compositions and code validation must be taken into account. To account for these uncertainties, the sum of biases and uncertainties is taken from the analysis upon which the models are based. These biases and uncertainties are not quantitively reevaluated, although they were rounded up to the nearest percent change in k_{eff} (% Δk_{eff}) to expedite the analysis. The models used for PWR NFV analysis are discussed in Section 2.3.1, and the models used for the BWR NFV analysis are discussed in Section 2.3.2. Both NFV models were full-scale with vacuum boundary conditions.

2.3.1 PWR NFV Model

The PWR NFV model used for the LEU+ sensitivity studies consisted of a concrete room with two racks, each capable of holding 35 fresh fuel assemblies in 7 × 5 arrays. Each assembly is supported by a rack cell with steel braces. Calculations varied the moderator density to account for the fully flooded and optimum moderation conditions. Concrete was modeled as the SCALE composition definition of US Nuclear Regulatory Commission-developed regulatory concrete (REGCONCRETE). The steel was modeled as SS316 stainless steel.

The assembly type used was the Westinghouse 17 × 17 Standard (W 17 × 17 STD) design [9], which has 25 fuel rod locations displaced by instrument and guide thimbles. The baseline model uses 5 wt % enriched UO_2 with a density of 10.41 g/cm^3 corresponding to 95% of theoretical density. The cladding and thimbles were composed of Zircaloy-4 as is representative of modern PWR fuel. Each of the NFV rack cells were modeled as an assembly within four stainless-steel L-shaped braces, which serve to support and maintain spacing between the assemblies. The NFV rack is modeled as two modules of 7 × 5 arrays of rack cells. The NFV racks are located within concrete walls. The NFV interior measures 589.28 × 1,173.48 × 518.16 cm, and the walls extend to 894.08 × 1,478.28 × 670.56 cm. The concrete walls and floor are modeled as having a uniform 152.4 cm thickness. No ceiling is modeled, and the top of the steel brace marks the upper boundary of the NFV model. Each 7 × 5 array of cells is placed 33.02 cm away from the left wall. The first array is placed 33.02 cm from the upper wall, and the second array is 35.56 cm below the first array. This results in the bottom left corner of each array being positioned at *xy* coordinates of (-261.62, 162.56) and (-261.62, -264.16), respectively, when the vault is constructed centered about (0, 0). The assemblies rest on the concrete floor. The pitch of 55.88 cm is notably greater than the size of an assembly. An accidental dropped assembly could therefore fit between the designated slots, and if mitigated in the design, was not noted.

Table 2 contains the W 17 × 17 STD assembly geometric parameters, and Table 1 contains the geometric parameters used to describe the NFV rack. Figure 1 provides a cross-sectional view of a fuel assembly in the PWR NFV rack cell. Figure 2 shows an isometric view of the PWR NFV model, and Figure 3 shows a cross-sectional view of the PWR NFV model. Both figures are rotated for visual purposes.

Table 2. W 17 × 17 STD nominal assembly geometric parameters. [9]

Specification	Value
Fuel radius	0.410 cm
Gap radius (clad IR)	0.418 cm
Clad outer radius	0.475 cm
Thimble inner radius	0.572 cm
Thimble outer radius	0.612 cm
Fuel rod/thimble pitch	1.260 cm
Fuel rod/thimble height	365.760 cm

Table 3. PWR NFV geometric parameters.

Specification	Value
Assembly pitch	55.88 cm
Number of thimbles	25
Steel brace thickness	0.635 cm
Steel brace height	518.16 cm
Steel brace length, width	5.08 cm
Steel brace inner dimension	11.43 cm

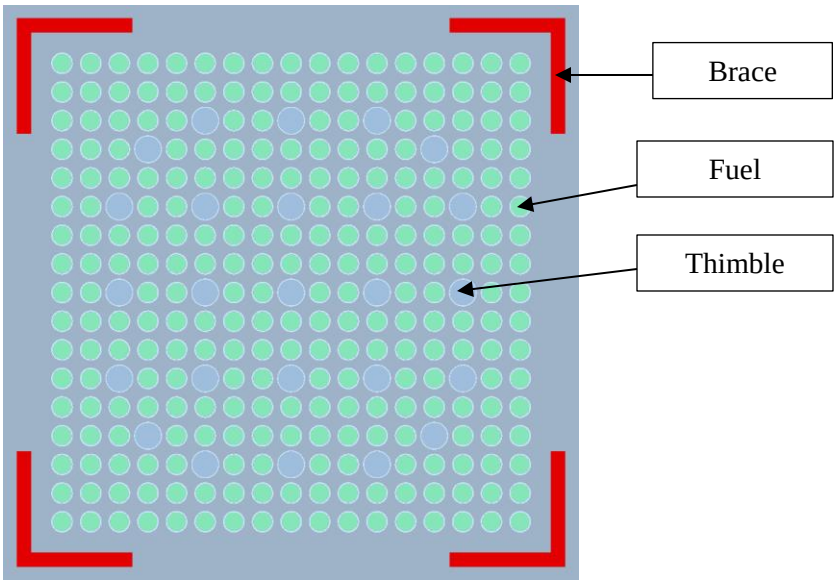

Figure 1. Cross-sectional view of the PWR NFV rack cell with W 17 × 17 STD fuel assembly.

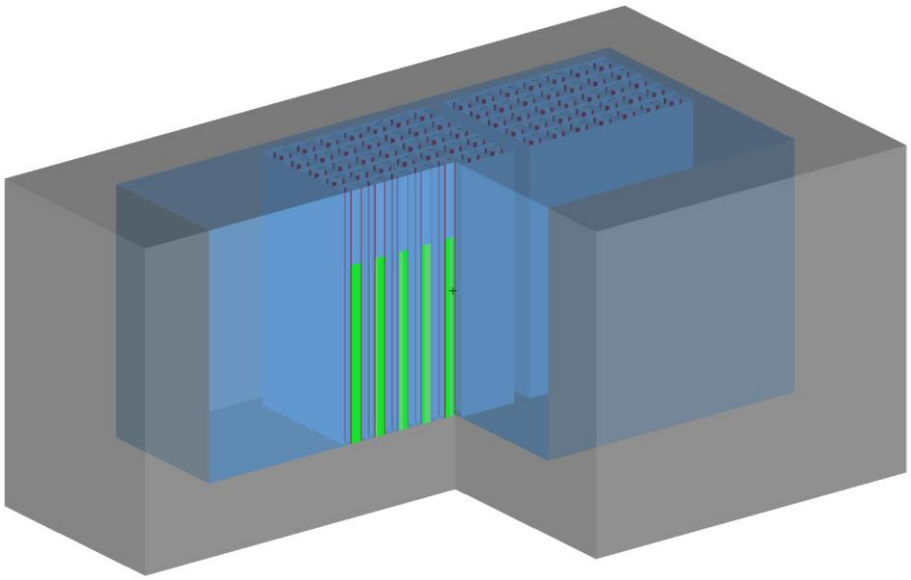

Figure 2. Isometric view of the PWR NFV model with the front right quarter removed.

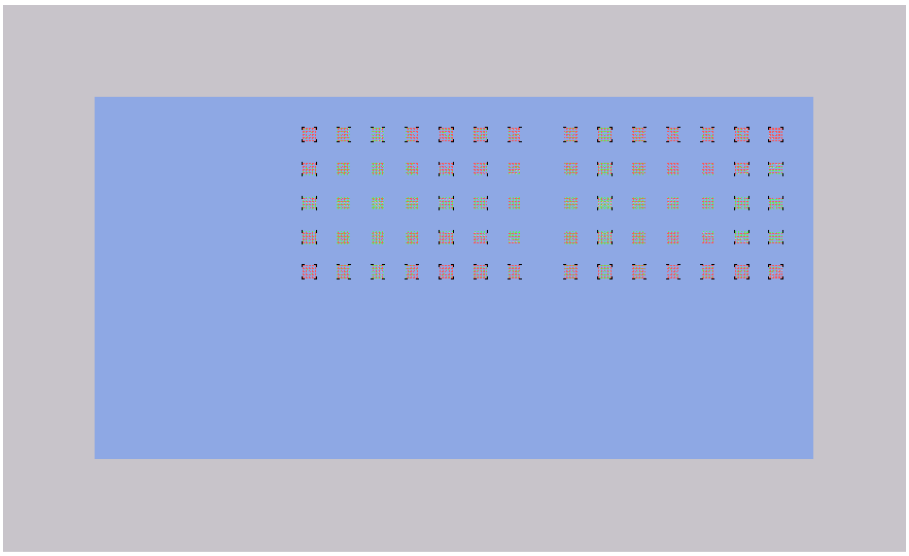

Figure 3. Horizontal cross section of PWR NFV model.

2.3.2 BWR NFV Model

The assembly type used for the BWR calculations is the ATRIUM 10 design [10], outlined in Table 4, which consists of a 10 × 10 array of fuel rods with nine empty spaces for a Zirc-2 central water channel. The baseline model fuel is 4.7 wt % enriched UO_2. The fuel density was modeled as 10.55 g/cm^3 corresponding to 96% the theoretical density of UO_2. The cladding, water channel, and fuel channel were composed of Zircaloy-2. The fuel assemblies also have a Zirc-2 fuel channel surrounding the fuel array. The baseline model also credits eight gadolinium (Gd)-bearing fuel rods, which contain 2 wt % Gd_2O_3. The fuel assemblies are supported and separated by SS304 stainless-steel braces. Table 6 provides the geometric parameters used to describe the NFV rack, and Figure 4 shows the layout of the baseline BWR NFV model at the assembly level.

Table 5. ATRIUM 10 fuel specification. [10]

Specification	Value
Fuel radius	0.433 cm
Gap radius (clad IR)	0.442 cm
Clad outer radius	0.503 cm
Fuel rod pitch	1.295 cm
Assembly height	381 cm
Fuel channel inner width	13.406 cm
Fuel channel thickness	0.254 cm

Table 6. BWR NFV geometric parameters.

Specification	Value
Assembly horizontal pitch	16.764 cm
Assembly vertical pitch	20.764 cm
Water channel inner width	3.355 cm
Water channel thickness	0.072 cm
Steel bracer inner width	16.12 cm
Steel bracer outer width	16.764 cm
Bracer gap width	6.0 cm

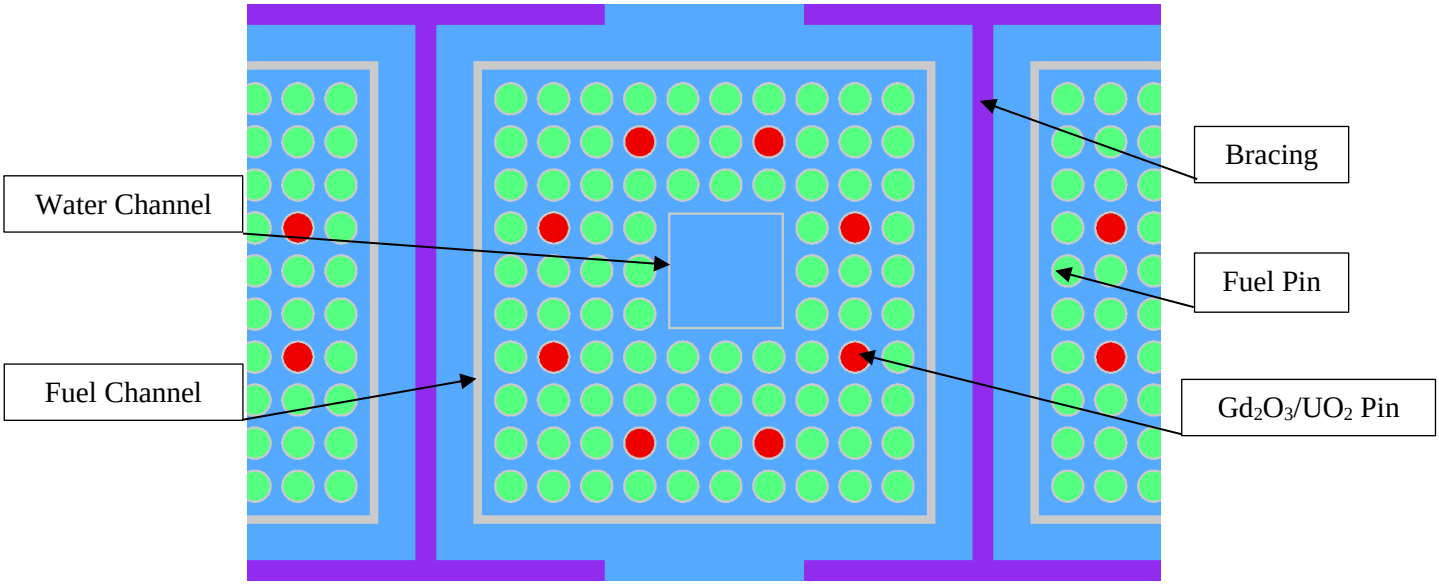

Figure 4. Horizontal cross-sectional view of BWR NFV rack cells.

The NFV was modeled with an array of 21 × 10 fuel assemblies flooded with water with the surrounding concrete structure. The vault interior dimensions of the NFV are 193.04 × 462.714 × 389.5852 cm, and the surrounding concrete extends to 248.92 × 518.594 × 420.0652 cm. The concrete walls are 27.94 cm thick. The floor is 30.48 cm thick with an 8.5852 cm gap between the storage cells and the floor. The top of the vault is aligned with the top of the storage cells. The 21 × 10 array is centered 12.7 cm from the left and right wall interiors, and 13.335 cm from the upper and lower wall interiors. Figure 4 shows the cell level details of the models, and Figure 5 and Figure 6 show an isometric view and horizontal cross section of the vault, respectively. Figures are rotated for visual purposes.

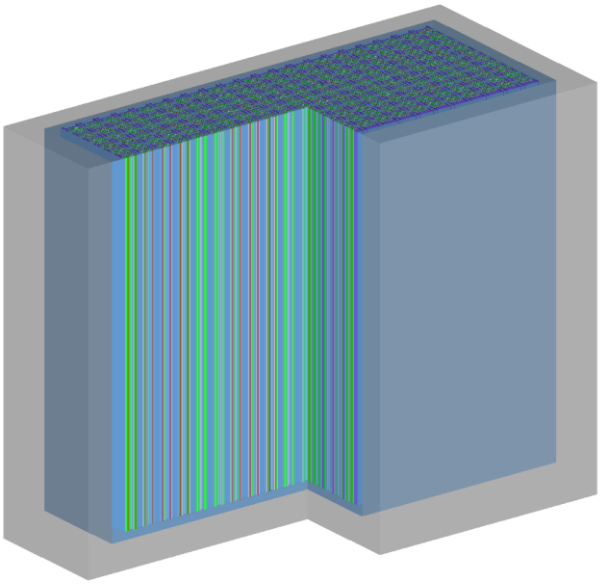

Figure 5. Isometric view of the BWR NFV with the front right corner removed.

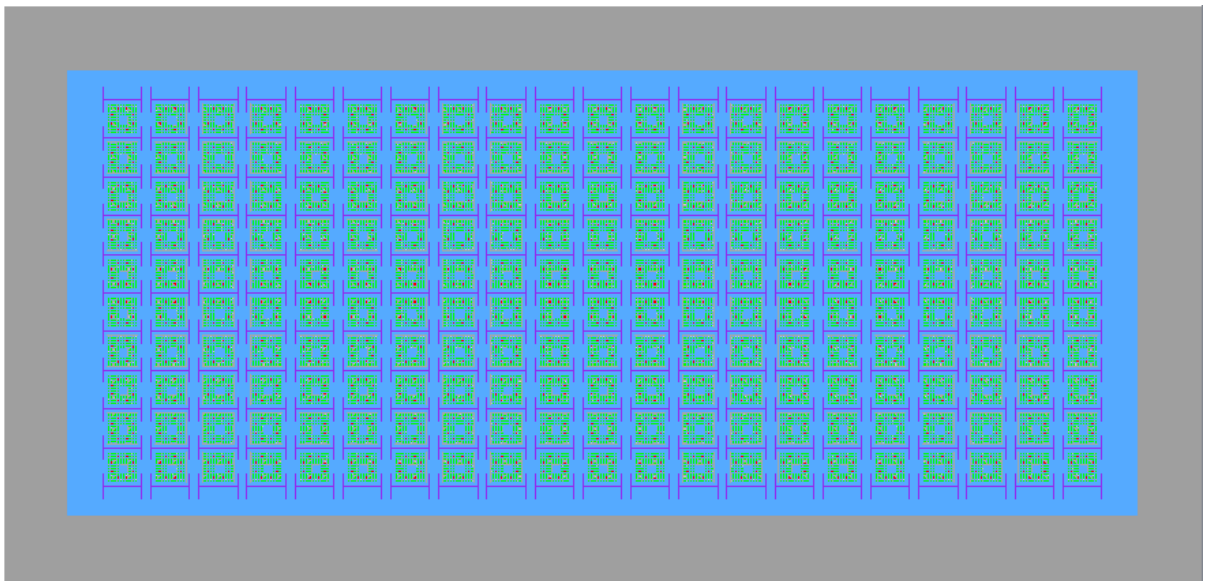

Figure 6. Horizontal cross section of BWR NFV model.

2.4 SPENT FUEL POOL ANALYSIS

The racks in SFPs are designed to accommodate fresh and spent fuel. In PWRs, there are typically racks used for high-density storage for burned fuel and racks used for low-density storage associated with fresh fuel that was staged in the SFP before being loaded in the core. This low-density storage can also be used to store fuel between cycles or in the event of an emergency core offload. For BWR SFPs, a homogenous pool loading typically accounts for the burnup which results in the maximum reactivity of a fuel assembly. This work is focused on criticality analysis of fresh fuel. Because the high-density PWR storage and BWR fuel analysis require the analysis of fuel burnup, they are not considered here and will be handled in a separate report.

SFP criticality analysis is done in compliance with 10 CFR 50.68 (4), as discussed in Section 2.2. In practice, 10 CFR 50.68 (4) establishes two limits for PWR SFPs: that k_{eff} is less than 1.0 for normal conditions without boron and less than 0.95 for normal and accident conditions when crediting the soluble boron in the SFP water. The sensitivity studies for SFP racks for LEU+ and ATF fuel consider both limits.

Low-density racks for PWR SFPs typically have a flux-trap design with each assembly stored in a stainless-steel compartment. The individual compartments are typically designed to have a water gap and two neutron absorber panels between the assemblies. Over time, some of the installed neutron absorbers in SFP racks degrade, resulting in plants modifying the criticality analysis of the SFP. To account for this, two rack designs were used to perform sensitivity studies: one with neutron absorber panels present and one where the neutron absorbers are assumed to have degraded and are not modeled. The SFP rack model with neutron absorbers present is referred to as the *intact absorber (IA) SFP model*, and the SFP model without neutron absorbers present is referred to as the *degraded absorber (DA) SFP model*.

In addition to the best estimate k_{eff} values calculated for each of these models, the reactivity biases and uncertainties due to the uncertainties in material dimensions and compositions and code validation must be taken into account. To account for these reactivity allowances, an estimated sum of biases and uncertainties was used. These biases and uncertainties were not specifically evaluated to expedite the analysis. The models used for PWR SFP analysis are discussed in Section 2.4.1. Both SFP models have periodic boundary conditions applied on the lateral faces of the 2 × 2 assembly array.

2.4.1 PWR SFP Models

Two models were used to examine the impact of a transition to LEU+ and ATF for PWR SFPs: an IA SFP model and a DA SFP model. Although both designs are similar in original construction, the neutron absorbers are assumed to degrade in the DA model and are assumed to remain intact in the IA SFP model. Because pools are large and have a repeated assembly layout, calculations were done with periodic radial reflection on 2 × 2 arrays of cells, as is typically done when analyzing SFPs.

The DA SFP model for LEU+/ATF sensitivity analysis consists of a 2 × 2 assembly array of SS316 rack cells with two fuel assemblies and two empty cells arranged in a checkerboard configuration. The W 17 × 17 STD assembly type with UO_2 was enriched to 5 wt % with a density of 10.52 gm/cm^3, corresponding to 96% of theoretical density. Table 8 provides the geometric parameters used to describe the DA SFP model, it is noted that the assembly parameters are the same as those provided in Table 7 for the PWR NFV model. Figure 7 shows a horizontal cross section of the PWR DA SFP model.

Table 8. PWR DA SFP rack model dimensions.

Specification	Value
Center-to-center spacing	27.305 cm
Cell inner dimension	22.606 cm
Cell wall thickness	0.305 cm
Cell wall height	518.16 cm

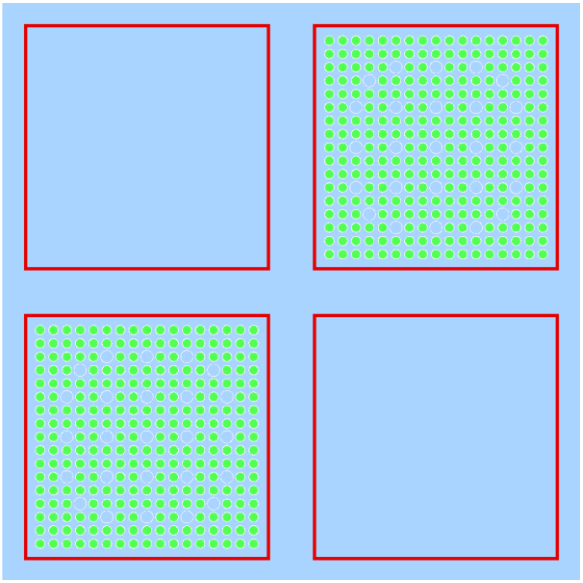

Figure 7. Horizontal cross section of the DA SFP model.

The IA SFP model is a 2 × 2 array of rack cells. The assemblies are centered within the rack cells with poison panels on each of the cell lateral faces. The design basis fuel used was a 5 wt % enriched W 17 × 17 STD assembly type with a UO_2 density of 10.686 gm/cm^3 corresponding to 97.5% of theoretical density. The cladding and thimble were composed of Zirc-4. Poison panels were defined as 70 wt % Al and 30 wt % B_4C resulting in an ^{10}B areal density of 0.0293 g/cm^2. To determine the effect of LEU+ enrichments on boron degradation effects, a study was performed examining k_{eff} as a function of areal density. The steel was modeled as SS316 stainless steel.

The stainless-steel rack cells have a 27.7622 cm center-to-center pitch with a 22.352 cm inner dimension and a 0.1905 cell wall thickness. The neutron absorber panels are centered on each face of the rack cell and are 19.05 cm wide. The absorber panels axially span the entire active length of the fuel with 5.08 cm of overhang on both ends. The poison panel is sheathed by a 0.0889 cm thick stainless-steel wrapper with a 0.03048 cm gap in between. Table 9 contains the geometric parameters used to describe the IA SFP assembly repeated in the 2 × 2 array positioning. Figure 8 shows a cross-sectional view of the IA SFP model. Vertical offset of the poison panel measures the distance between the bottom of the poison panel and the bottom of the assembly.

Table 9. PWR IA SFP assembly geometry.

Specification	Value
Center-to-center spacing	27.762 cm
Cell inner dimension	22.352 cm
Cell wall thickness	0.191 cm
Cell height	506.73 cm
Poison panel width	19.05 cm
Poison panel thickness	0.269 cm
Poison panel height	436.88 cm
Poison panel vertical offset	15.748 cm
Panel wrapper gap	0.030 cm
Wrapper thickness	0.089 cm
Neutron absorber B_4C loading	30 wt %

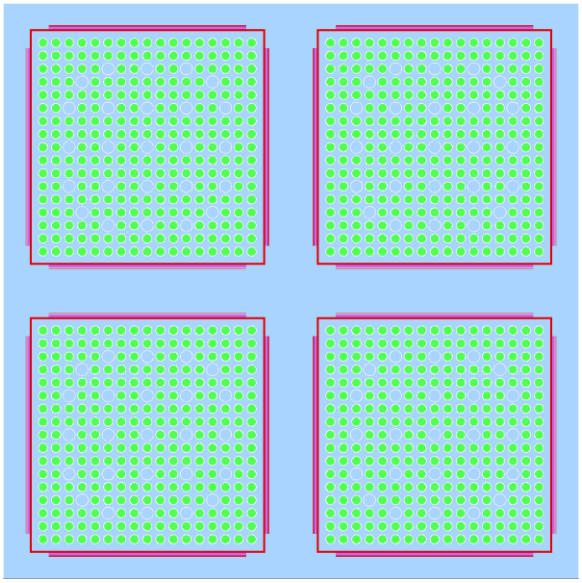

Figure 8. Horizontal cross-sectional view of the IA SFP model.

2.4.2 Accident Analysis and Soluble Boron Credit Models

Evaluating accident conditions is an essential component of criticality analysis. In SFPs, the reactivity associated with accidents is mitigated with soluble boron credit (SBC) in which the boron dissolved in the SFP water can be used to offset reactivity increases from abnormal conditions. Typically, the accident in which a fuel assembly is misloaded into a storage location that is required to be empty under normal conditions results in the greatest reactivity increase. If fuel with greater than 5.0 wt % enrichment is

incorporated into fuel management, then the misload accidents will result in more reactive configurations than are currently considered.

To investigate the impact of LEU+ enrichments on soluble boron requirements, a series of misload calculations was performed by using the DA SFP rack model. The DA SFP configuration requires that the fresh fuel assemblies be stored in a checkerboard configuration of fuel and empty storage locations under normal conditions. The use of physical distance between assemblies as a reactivity control in this manner results in the potential to achieve a more reactive state than can be accomplished with the IA model (i.e., the IA model is intended to be fully loaded, and thus misplacement is less consequential).

The first step in modeling the misload calculations was to expand the 2 × 2 array of cells to 10 × 10 to reduce the periodic boundary condition effects upon introducing new assemblies. The misload calculations were then performed by incrementally filling the locations that are intended to be empty. To determine the effects of LEU+ enrichments on soluble boron requirements, multiple hypothetical misloading scenarios were considered as to examine the potential enrichment dependent effects. The left portion of Figure 9 depicts the 10 ×10 array of DA SFP rack model cells before misloading, and the right portion shows the model with 11 misloaded assemblies with each incremental misload identified (i.e., the cell marked "1" was the first misload, the cell marked "2" was the second additional misload, etc.). Misloads were clustered together to maximize the effect. Burnable absorbers credit was not considered. The calculations were performed with the baseline 5.0 wt % enrichment, as well as the LEU+ enrichments of 6.5 and 8.0 wt %. Models were further adjusted to incorporate soluble boron in the pool, calculating the boron concentration required to demonstrate compliance with regulation upon misloading. Boron concentrations ranged up to 2,000 ppm, with operational ranges between 2000 and 2500 ppm not uncommon at 5 wt %. The array before and after misloading is shown in Figure 9.

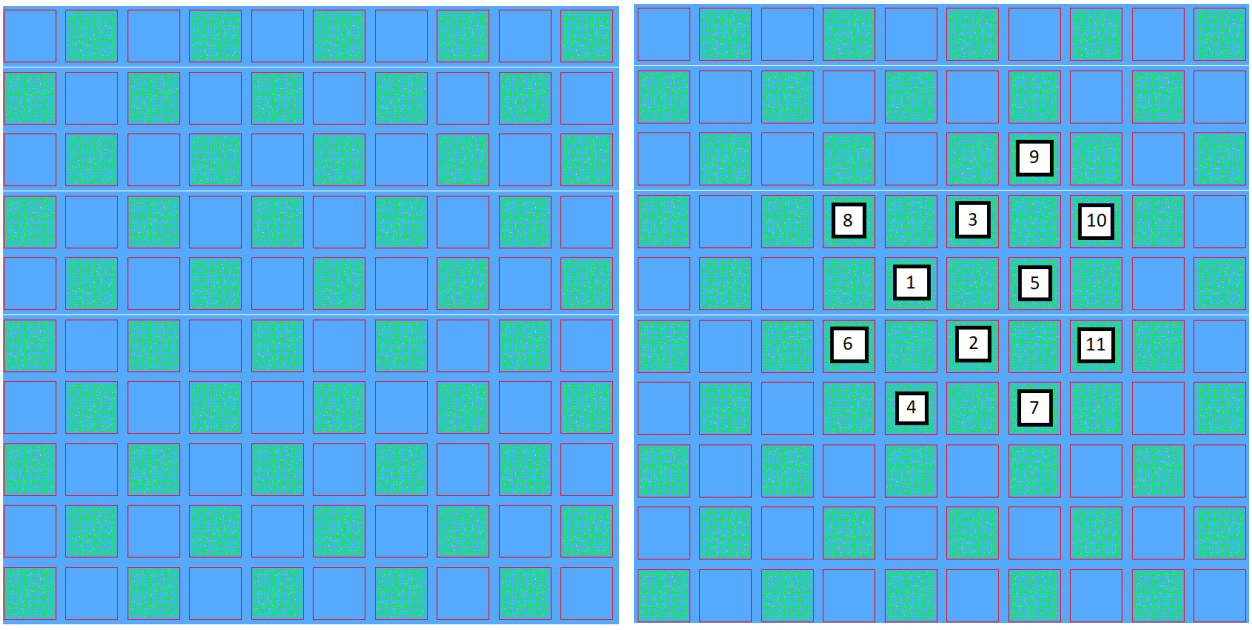

Figure 9. Expanded PWR DA SFP model used to evaluate misload configuration and soluble boron calculations.

2.5 ACCIDENT TOLERANT FUEL CONCEPTS

This work also examined the reactivity impact on fresh fuel of ATF concepts. ATF options examined in this work include Cr-coating of the conventional Zirc-4 cladding (Cr-coated), Cr_2O_3 (Chromia) doping of

the UO_2 fuel (Cr-doped), and the use of iron-chromium-aluminum (FeCrAl) cladding. ATF parameters, including composition and dimensions, were taken from compiled values reported in Hall et al. [11] for reported ATF concept parameters in various stages of industry testing.

The Cr-coating on the fuel rod was 20 μm thick and was composed entirely of elemental chromium. The thickness was chosen to fall within the potential ranges of both Westinghouse and Framatome implementations, as reported in Hall et al. [11], and so a 0.002 cm layer of Chromium was added to the nominal fuel cladding thicknesses. Only the fuel cladding—not the fuel or water channel made of zirconium, had this extra layer of Chromium. Chromium layered cladding is of interest for reducing zirconium-water reactions at high temperatures. Given the thin layer of relatively neutronically transparent chromium, little neutronic impact was anticipated.

Chromia fuel-doping parameters are proprietary among vendors, although experimentation with Westinghouse ADOPT fuels has given some insight into potential doping schemes [11]. One such experiment was done with 1,000 ppm Cr_2O_3 by weight, which was subsequently modeled as a fuel volume fraction of 0.001 with a constant density. Chromia is not included in the SCALE standard composition library of materials, so Chromia was modeled as 680 ppm Cr by weight and 320 ppm O. In gadolinia rods, the fuel was treated as 97.9% UO_2, 2 % gadolinia, and 0.1% chromia. Introducing metal oxide dopant increased fuel grain size and density. In minor concentrations, there is little neutronic penalty, whereas fuel irradiation results in a more consistent density as a function of burnup; in effect, less void is available for settling.

Although multiple variations of alloys are considered FeCrAl and a production-ready design not yet revealed, several are known to have been implemented in test facilities [11] with the C26M variant reported to be among the most employed. As a result, the C26M variant of FeCrAl and its composition of 12% by weight Cr, 6% Al, 2% Mo, 0.2% Si, 0.003% Y, and the remainder Fe were modeled. FeCrAl allows for and necessitates thinner cladding and thicker fuel pellets because of its greater mechanical strength and neutron absorption relative to standard Zr-based cladding. The fuel pellet radius and cladding inner radius increased by 0.018925 cm while preserving the cladding outer radius, increasing from 0.409575 and 0.41783 cm to 0.4285 and 0.436755 cm for PWR fuels and from 0.433451 and 0.44196 cm to 0.452376 and 0.460885 cm for BWR fuels.

2.6 OTHER MODELING CONSIDERATIONS IN ONSITE FUEL STORAGE

Several analyses or assumptions are commonly relied upon in the performance of fuel storage criticality analyses. LEU+ enrichments present potential challenges to long-held margins and underlying assumptions. This section discusses the methods used to evaluate some of these analyses or assumptions.

2.6.1 Neutronic Decoupling Distance Evaluation

Static storage of fuel assemblies is not the only operation that occurs in SFPs. Other operations include moving fuel assemblies around the pool and inspecting fuel assemblies. Many of these operations involve moving an assembly around the SFP but not in close proximity to other fuel assemblies. When assemblies are separated by enough water, the neutrons from one cannot cause fission in another. These assemblies are assumed to be isolated or neutronically decoupled. Many of the normal operating and accident conditions discussed in NEI 12-16 [12] are judged to be neutronically decoupled when at least 12 in. (30.48 cm) of water separates the assemblies. This study investigated whether this assumption is valid for the baseline and LEU+ configurations analyzed in Section 2.3.

The sensitivity of the neutronic decoupling distance to enrichment was investigated by running a series of calculations in which the distance between the assemblies was varied. The calculations were performed

for the ATRIUM 10 and W 17 × 17 STD assemblies. The center-to-center distance was varied from 20 to 100 cm for the ATRIUM 10 assembly design, resulting in edge-to-edge distances varying from 6.08 to 86.08 cm. The center-to-center distance was varied from 30 to 100 cm for the W 17 × 17 STD assembly design, resulting in edge-to-edge distances varying from 8.58 to 78.58 cm. For each assembly design, the k_{eff} value for the distance of maximum separation was subtracted from each of the k_{eff} values with less separation.

2.6.2 Eccentric Positioning Analysis

NFV and SFP racks are designed to maintain the separation of fuel assemblies and are nominally modeled with the assemblies in the center of cells. However, where the assemblies are placed within the storage cell is not controlled, and clearance between the assembly and cell is needed to allow for insertion and withdrawal without damaging the fuel assembly. Off-center positioning or eccentric positioning of the assemblies could cause clustering of assemblies within their racks and result in a more reactive state than fully centered assemblies. To investigate this effect and the effect that LEU+ enrichment would have on the reactivity impact of such positioning, the NFV and SFP models were offset in a clustered manner to observe any reactivity deviations. These positionings are presented in Figure 10Figure 13. Although many permutations could be examined in these arrays of racks, the chosen positioning is believed to be reasonable to determine whether there is an enrichment-dependent effect on eccentric positioning calculations. Internally within the racks, assemblies were moved the maximum distance to the cell wall. Generally, assemblies were shifted one of the four ordinal directions so that the array would be centrally clustered (best shown in Figure 12). PWR SFP models were expanded to 4 × 4 cell arrays, as recommended in NEI 12-16 [12]. For each of the cases considered in this report, slightly different eccentric positioning scenarios based on the rack layout were used. The BWR NFV model uses the entire NFV geometry with all assemblies positioned toward the center of the NFV. In the PWR NFV eccentric positioning model, assemblies within each of the 5 × 7 modules are moved toward the center of the module along the diagonal. In the PWR IA eccentric positioning model, the assemblies are moved toward a center point in the middle of the 4 × 4 array. In the PWR DA SFP model, each of the assemblies in the 4 × 4 array are moved toward the two assemblies on the centerline, which are placed in the center of the cell. The eccentric positioning model is shown for the BWR NFV model in Figure 10, the PWR NFV in Figure 11, the IA SFP model in Figure 12, and the DA SFP model in Figure 13. The orange arrows in all the eccentric positioning figures indicate the direction of the eccentric position of the assembly in that cell.

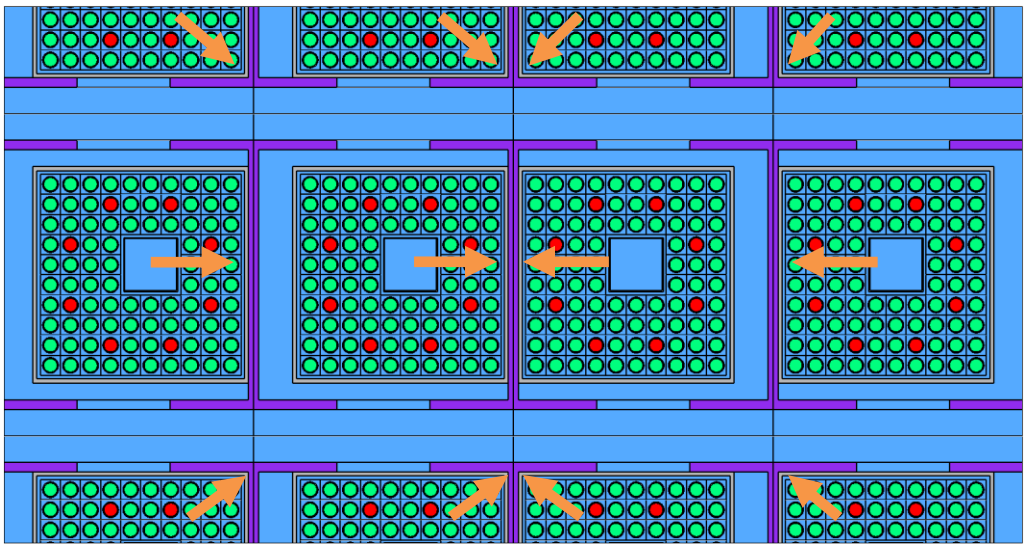

Figure 10. BWR NFV eccentric positioning map.

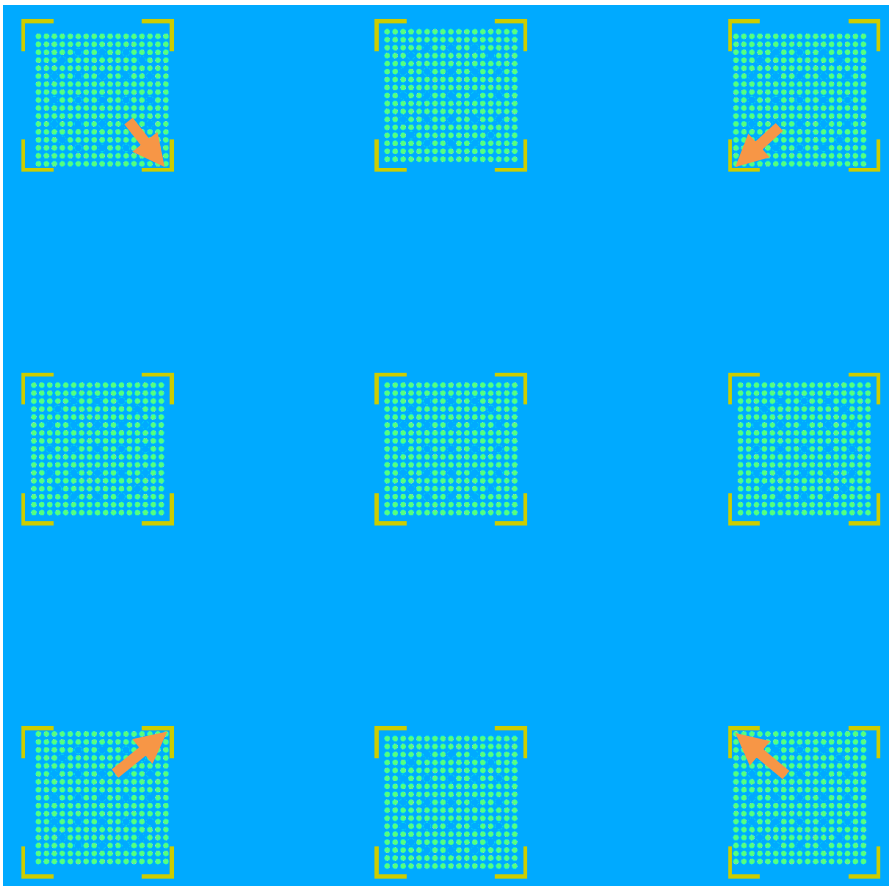

Figure 11. PWR NFV eccentric positioning map.

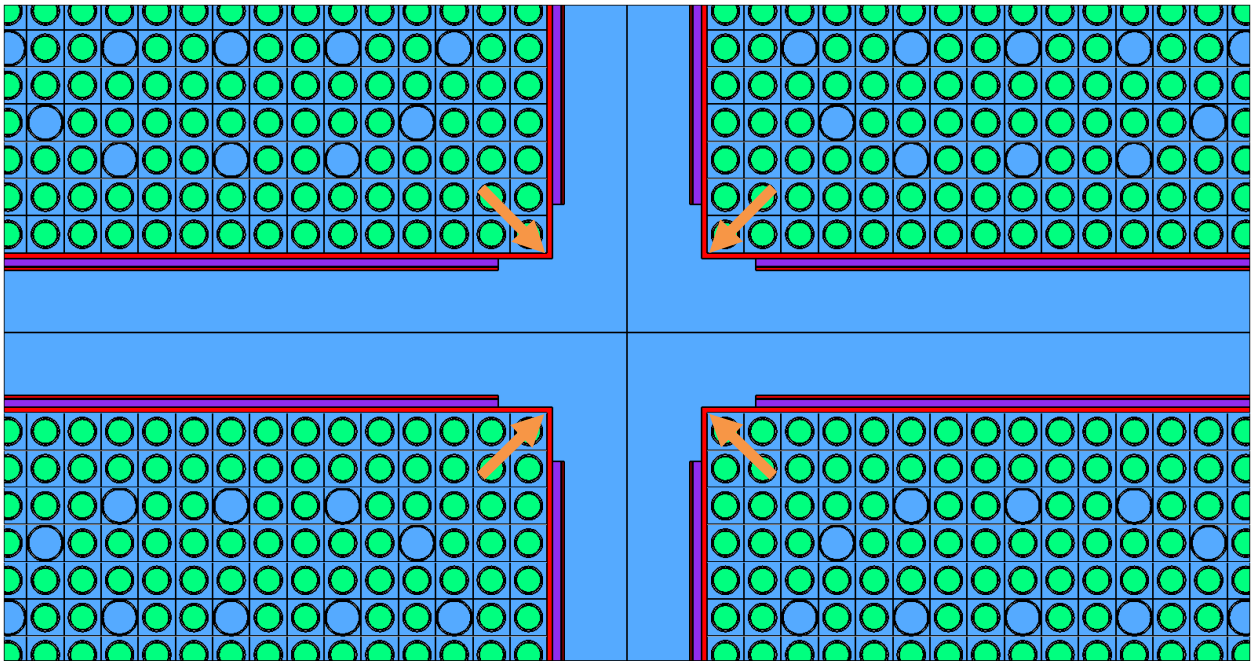

Figure 12. PWR IA SFP eccentric positioning map.

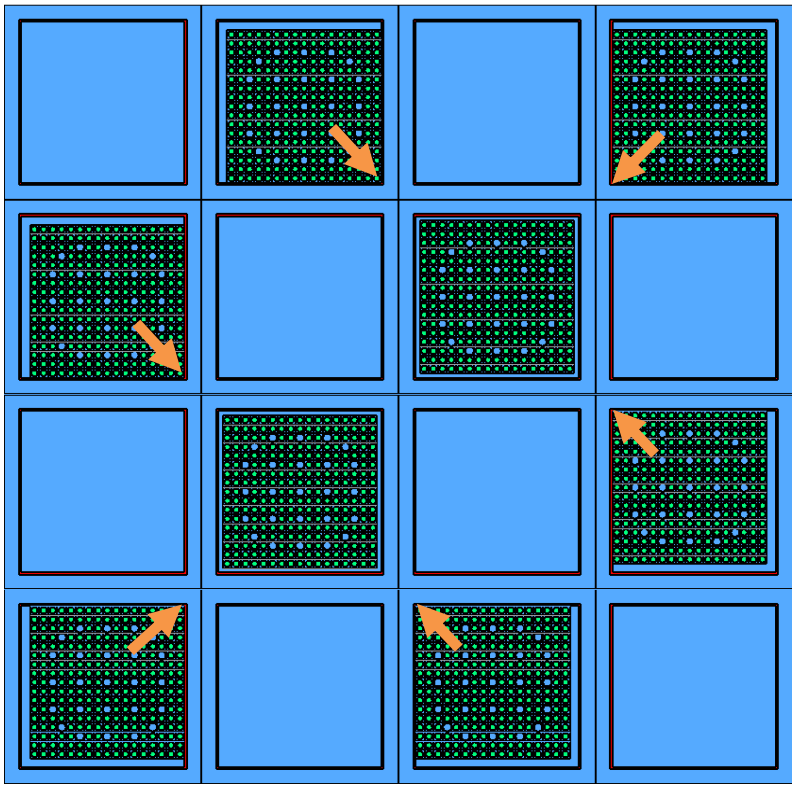

Figure 13. PWR DA SFP eccentric positioning map.

2.7 RADIAL ENRICHMENT ZONING STUDY

Some fuel designs have multiple radial enrichments in a lattice design to flatten the in-core radial power distribution. It is typically expedient to model assemblies with radial enrichment zoning as having a single lattice average enrichment. It is desirable to confirm the conservatism of this approach and to examine the sensitivity of this assumption to LEU+ enrichments. The assembly designs with the greatest degree of radial heterogeneity are BWR assemblies. A publicly available, detailed description of a GE 14 BWR lattice was provided in Fensin [13]. To investigate the impact of radially averaging the enrichment, two dominant lattice calculations were performed, as described in Fensin [13]. The first calculation used the full radial detail, including modeling the pin enrichments and Gd_2O_3 loadings. The calculation modeled each pin as having an enrichment corresponding to the assembly. The second calculation retained that pin-wise Gd_2O_3 loadings from the pin-wise model. The dominant lattice in Fensin [13] had an average enrichment of 4.3 wt %, which was increased to 6.5 and 8.0 wt % to investigate the effect of increased enrichment on the conclusions of the lattice average enrichments. The individual pin-wise model enrichments were fractionally increased to be consistent with the lattice average values. The lattices used in the calculations are shown in Figure 14. The study was conducted by using the BWR NFV model discussed in Section 2.3.2. For each lattice-averaged enrichment, the results between the pin-wise and lattice-averaged models were compared.

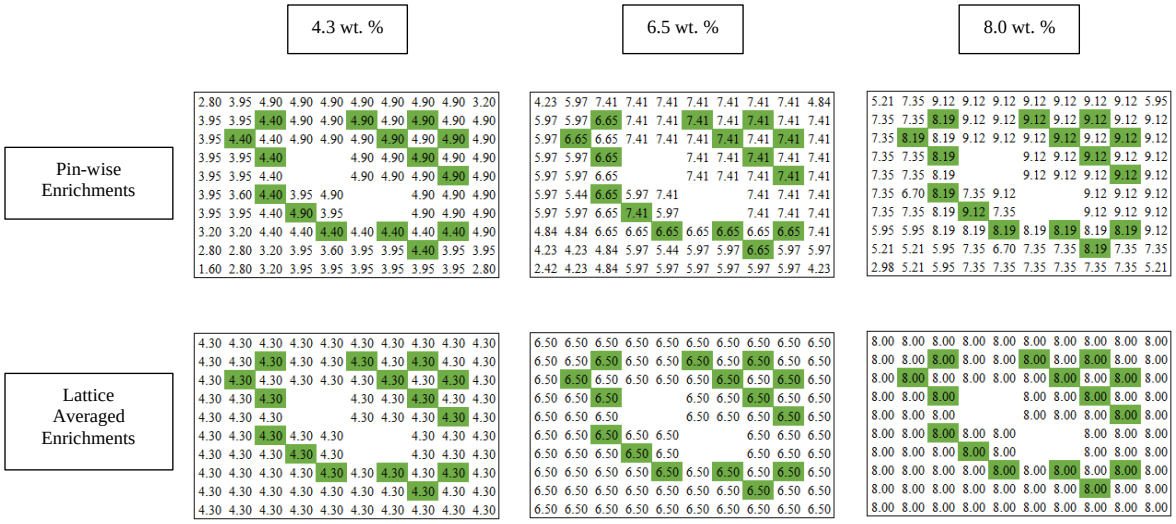

Figure 14. Lattices used in the radial enrichment zoning study.

2.8 ASSEMBLY CLUSTERING CALCULATIONS

Knowing the minimum number of assemblies needed to obtain a critical configuration as a function of enrichment can be beneficial. Arrays of ATRIUM 10 and W 17 × 17 STD assemblies were used to determine the impact of clustering assemblies together. Arrays of up to 9 ATRIUM 10 fuel assemblies (Figure 15) and up to 4 W 17 × 17 STD assemblies (Figure 16) were considered. Enrichments considered in the evaluation are the baseline values of 4.7 wt % for the ATRIUM 10 fuel and 5.0 wt % for the W 17 × 17 STD fuel and LEU+ enrichments of 6.5 and 8.0 wt % for both fuel types. All calculations were run assuming the assemblies are immersed in full density fresh water. The ATRIUM 10 calculations were performed by using eight rods, each containing 2 wt % Gd_2O_3. The W 17 × 17 STD calculations were performed by using 0, 32, and 64 integral fuel burnable absorber (IFBA) rods to account for the possible variation in minimum absorber loadings that might be seen in future operations.

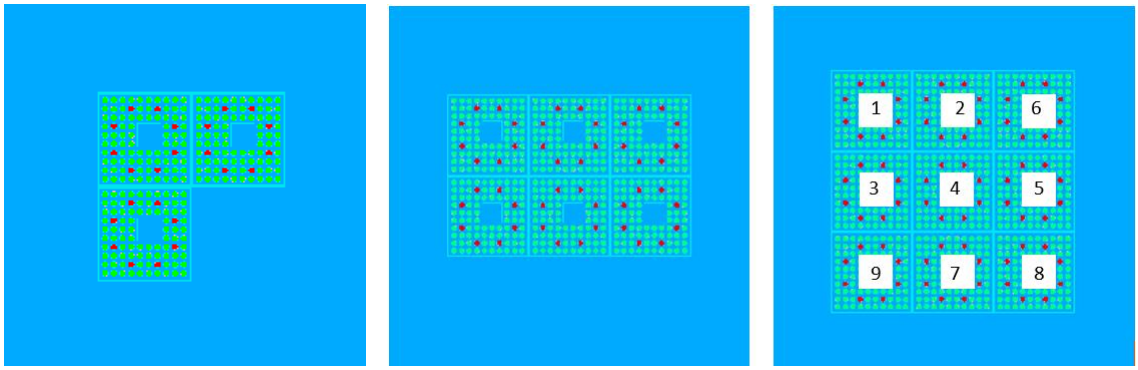

Figure 15. Examples of ATRIUM 10 assembly clustering models.

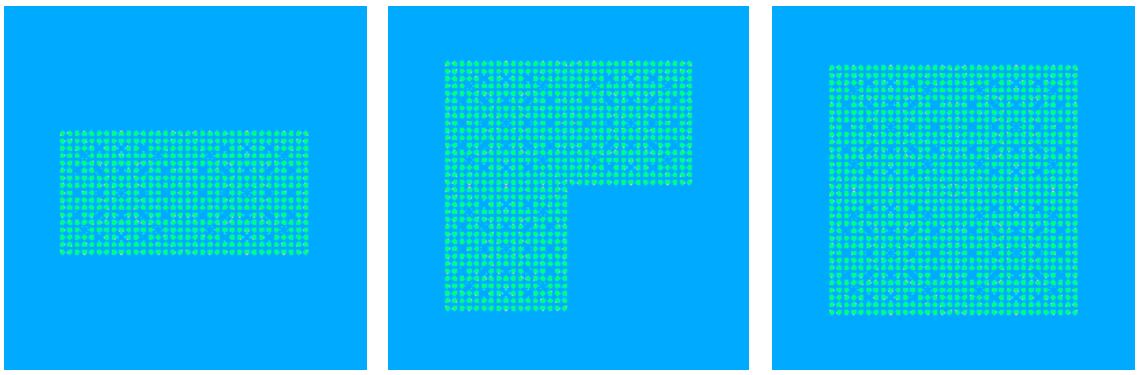

Figure 16. Examples of W 17 × 17 STD assembly clustering models.

3. RESULTS

3.1 PWR NFV

3.1.1 Fully Flooded

For the fully flooded condition, the baseline NFV model filled void in the vault with water at nominal density. Table 10 provides the results for the fully flooded baseline 5% enrichment, as well as the LEU+ enrichments of 6.5 and 8%. The standard Zr cladding and UO_2 fuel are the limiting conditions for this fuel vault for all enrichments. Figure 17 shows a bar graph of these values relative to the nominal fuel design of 5 wt% Zirc-4 case. The regulatory limit of 0.95 is accounted for with the black bar, which is also relative to the nominal case. For each case, a sum of biases and uncertainties was assumed to be 0.02 Δk_{eff} (an increase over FSAR reference values, as bias and uncertainties cannot be evaluated here) and included in reported maximum k_{eff} values. Notably, most conditions exceed the regulatory limit of 0.95 for LEU+ fuel designs.

Table 10. Maximum k_{eff} for fully flooded PWR NFV.

	ATF cladding material			
Fuel enrichment (wt %)	**Zirc-4**	**Cr-coated**	**Cr-doped**	**FeCrAl**
5.0	0.9429	0.9373	0.9426	0.9085
6.5	0.9767	0.9716	0.9766	0.9473
8.0	1.0003	0.9955	1.0001	0.9746

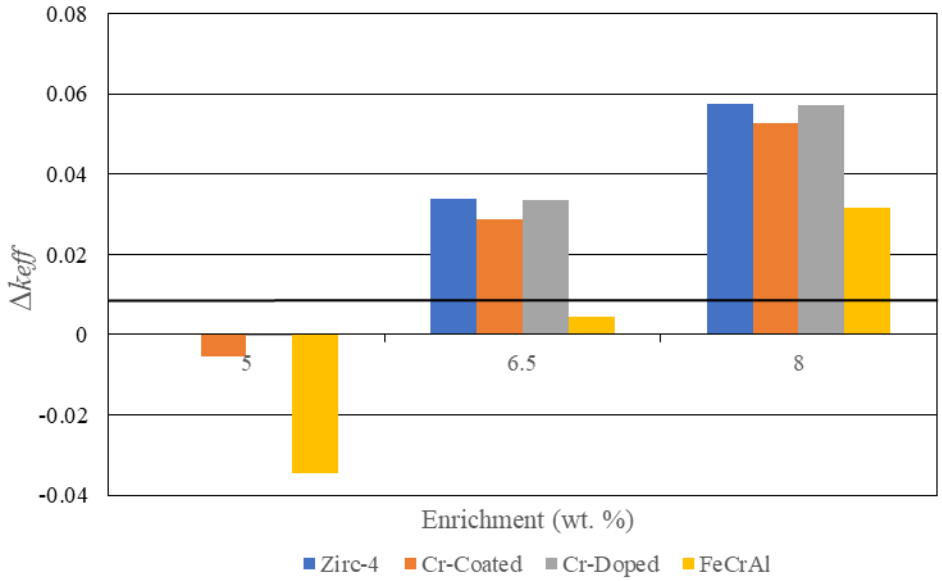

Figure 17. Changes from the baseline of the LEU+ and ATF changes for the fully flooded PWR NFV model.

The differential changes of LEU+ and ATF fuel forms from the baseline are shown in Figure 17. The results in Figure 17 show that the increase from 5.0 to 6.5 wt % results in a ~0.034 Δk_{eff} increase, and the increase from 5.0 to 8.0 wt % results in an increase of ~0.057 Δk_{eff}. The impact of the Cr-coated cladding is ~0.005 Δk_{eff}, and the impact of the Cr-doped fuel form is negligible, regardless of enrichment. The FeCrAl shows a significant suppressive effect that is enrichment dependent. The effect of the FeCrAl fuel form is ~0.034 Δk_{eff} for the 5.0 wt % case, ~ 0.03 Δk_{eff} for the 6.5 wt % case, and ~ 0.026 Δk_{eff} for the 8 wt % case.

3.1.2 Optimum Moderation

To determine the water density corresponding to optimum moderation, a series of calculations was performed by varying the water density throughout the vault from 1 to 90% (100% water density is addressed by the fully flooded condition) in increments of 10%. Based on these calculations, optimum water density was determined to be near 10%. To further refine the calculations, additional densities of 1, 5, 6, 7, 8, and 9% were modeled to find the exact peak. The curve is shown in Figure 18. The regulatory limit is 0.95 at fully flooded and 0.98 at optimum moderation. For each case, a sum of biases and uncertainties was assumed to be 0.02 Δk_{eff}. These calculations were performed for the baseline Zirc-4 cladding and the ATF types considered here. Table 11 reports the maximum k_{eff} for the optimum moderation condition by ATF concept, and the relative changes are presented in Figure 19. The point of optimum moderation occurred at 8% moderator density in all cases with the Zirc-4 UO_2 being the limiting condition.**Error! Reference source not found.** Figure 18 shows that there is no apparent change in the shape of the reactivity response to the change in moderation regime as a function of enrichment.

Table 11. Maximum k_{eff} for optimum moderation (8% moderator density) PWR NFV.

	ATF cladding material			
Fuel enrichment (wt %)	**Zirc-4**	**Cr-coated**	**Cr-doped**	**FeCrAl**
5.0	0.9101	0.9071	0.9098	0.8826
6.5	0.9502	0.9475	0.9496	0.9277
8.0	0.9798	0.9776	0.9796	0.9610

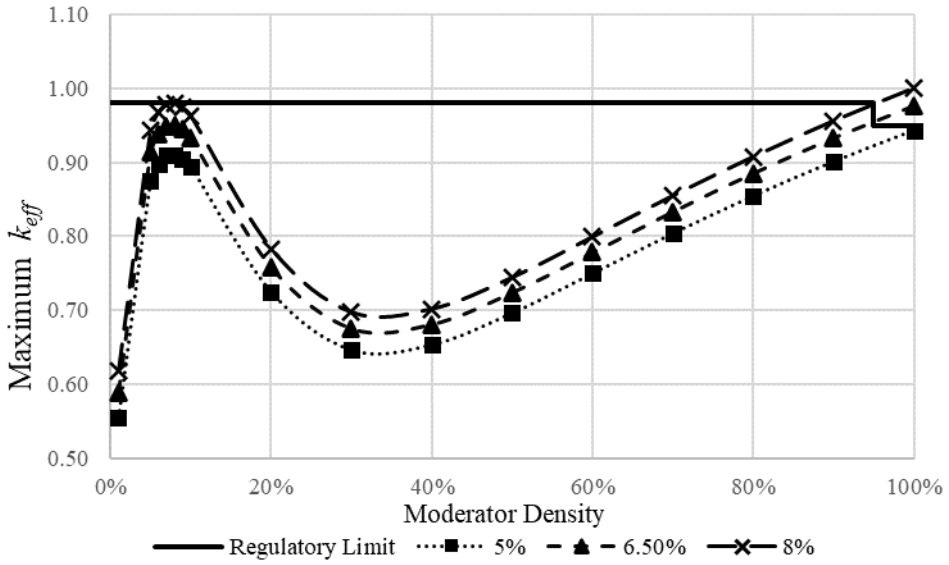

Figure 18. PWR NFV maximum k_{eff} as a function of moderator density.

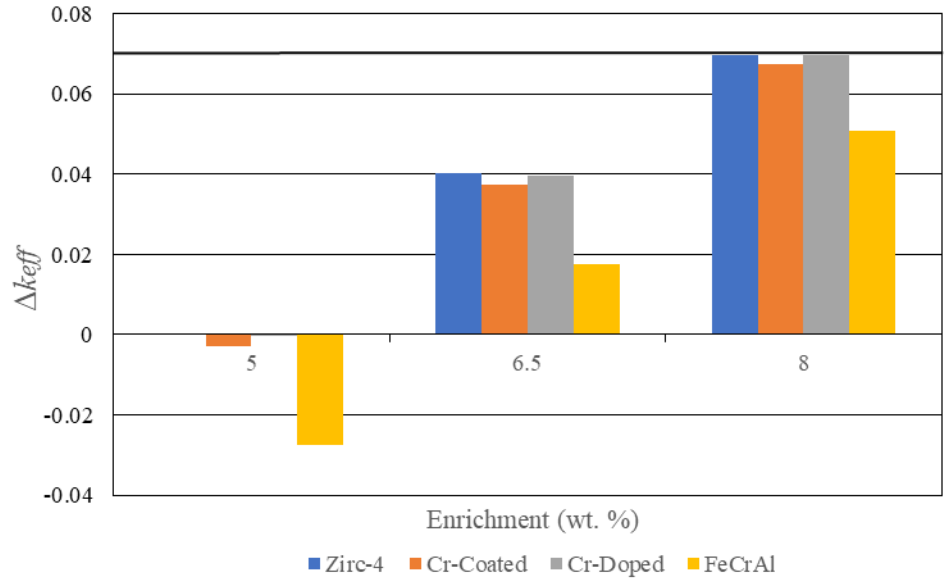

Figure 19. Changes from the baseline of the LEU+ and ATF changes for the optimum moderation PWR NFV model.

The differential changes of LEU+ and ATF fuel forms from baseline optimum moderation case are shown in Table 11. The results in Table 11 show that the increase from 5.0 to 6.5 wt % results in a ~0.04 Δk_{eff} increase, and the increase from 5.0 to 8.0 wt % results in an increase of ~0.07 Δk_{eff}. The impact of the Cr-coated cladding is ~0.003 Δk_{eff}, and the impact of the Cr-doped fuel form is negligible, regardless of enrichment. The FeCrAl fuel from shows a significant suppressive effect that is enrichment dependent. The effect of the FeCrAl fuel form is ~0.028 Δk_{eff} for the 5.0 wt % case, ~ 0.023 Δk_{eff} for the 6.5 wt % case, and ~ 0.019 Δk_{eff} for the 8 wt % case.

Figure 20 shows the difference between the full-density k_{eff} and the partial-density k_{eff} values for the 8 wt % enrichment case with each of the ATF fuel forms. The results in Figure 20 show that the ATF type barely influences the density-dependent behavior of k_{eff}.

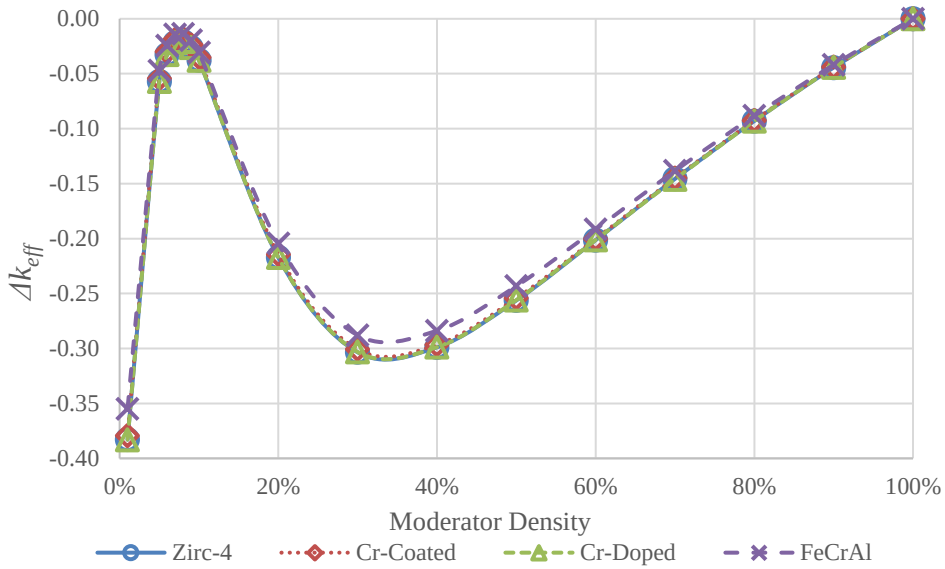

Figure 20. PWR NFV 8 wt % ATF Δk_{eff} relative to fully flooded.

Given the variable neutronic conditions across the range of moderator densities, the difference between the multigroup and continuous energy cross sections as a function of moderator density was investigated. Table 12 presents continuous-energy k_{eff} values and the difference between the multigroup and continuous energy k_{eff} values (calculated as CE – MG). Notably, in Table 12, there is a difference between the MG and CE calculations of approximately 300 pcm at decreased moderator densities; however, under these conditions, the multigroup predictions are higher, more conservative, k_{eff} values compared with the higher fidelity continuous energy cross section treatment. The difference between the calculations is on the order of MC uncertainty above 40 % moderator density. Figure 21 plots the behavior of each enrichment's multigroup bias with moderator density.

Table 12. PWR NFV multigroup bias as a function of moderator density.

Moderator density (%)	5% k_{eff}	5% MG bias (pcm)	6.5% k_{eff}	6.5% MG bias (pcm)	8% k_{eff}	8% MG bias (pcm)
1	0.5324	-213	0.5668	-199	0.5953	-203
5	0.8519	-277	0.8912	-248	0.9207	-256
6	0.8756	-253	0.9151	-274	0.9449	-274
7	0.8863	-253	0.9261	-250	0.9560	-263
8	0.8874	-261	0.9274	-277	0.9572	-260
9	0.8817	-279	0.9215	-290	0.9513	-281
10	0.8710	-256	0.9107	-264	0.9401	-258
20	0.7027	-238	0.7358	-255	0.7608	-233
30	0.6250	-153	0.6536	-178	0.6752	-164
40	0.6329	-80	0.6601	-96	0.6808	-63
50	0.6760	-44	0.7037	-32	0.7238	-20
60	0.7298	-5	0.7583	20	0.7789	-3
70	0.7840	19	0.8135	15	0.8347	3
80	0.8348	37	0.8657	41	0.8877	37
90	0.8814	60	0.9139	75	0.9366	57
100	0.9233	41	0.9574	66	0.9809	52

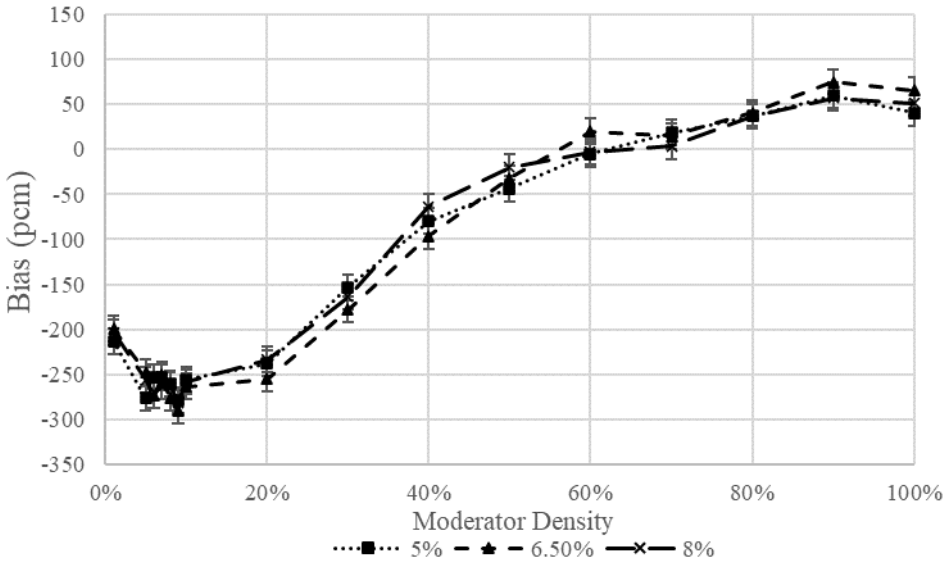

Figure 21. PWR NFV multigroup bias as a function of moderator density.

3.2 PWR POOL LEU+ AND ATF RESULTS

This section provides the sensitivity analysis for the unborated PWR spent fuel configurations. KENO V.a calculations were performed with the baseline PWR IA and DA SFP models by using 5.0 wt %. The calculated results for these configurations are a k_{eff} of 0.90776 for the IA model and 0.92116 for the DA model. For each case, a sum of biases and uncertainties was assumed to be 0.02 Δk_{eff} (an increase over FSAR reference values, as bias and uncertainties cannot be evaluated here). For each enrichment, the Cr-coated, Cr-doped, and FeCrAl ATF concepts were considered in addition to the baseline model. For each

case, the maximum k_{eff} was calculated by adding the sum of biases and uncertainties to the nominal k_{eff}. The reactivity change from the baseline was calculated by subtracting the 5.0 wt % case from each of the perturbed calculations. The maximum k_{eff} values are reported in Table 13 for the IA PWR SFP configuration and in

Table 14 for the DA PWR SFP configuration. The reactivity changes relative to the baseline configurations are reported in Figure 22 for the IA PWR SFP configuration and in Figure 23 for the DA PWR SFP configuration. In Figure 22 and Figure 23, the black line indicates how much k_{eff} margin is available to the regulatory limit of 1.0 for the unborated condition in the baseline case to provide a sense of the reactivity increases that could be tolerated without modifying hardware.

Table 13. Maximum k_{eff} values for the IA PWR SFP model.

	ATF cladding material			
Fuel enrichment (wt %)	**Zirc-4**	**Cr-coated**	**Cr-doped**	**FeCrAl**
5.0	0.9278	0.9219	0.9275	0.8962
6.5	0.9667	0.9612	0.9665	0.9397
8.0	0.9945	0.9893	0.9942	0.9711

Table 14. Maximum k_{eff} values for the DA PWR SFP model.

	ATF Cladding Material			
Fuel enrichment (wt %)	**Zirc-4**	**Cr-coated**	**Cr-doped**	**FeCrAl**
5.0	0.9412	0.9355	0.9409	0.9065
6.5	0.9766	0.9714	0.9763	0.9469
8.0	1.0012	0.9966	1.0009	0.9754

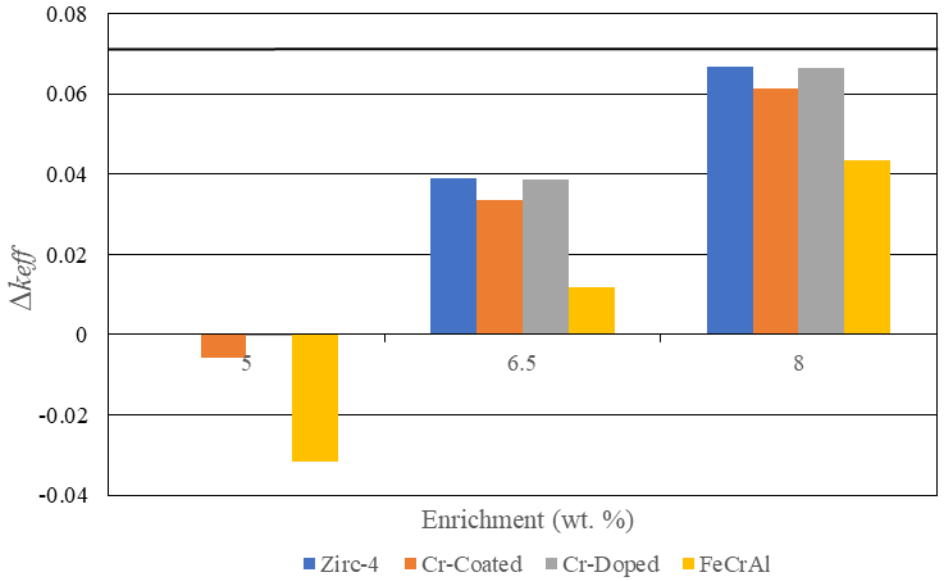

Figure 22. Changes from the baseline of the LEU+ and ATF changes for the PWR LD SFP IA model.

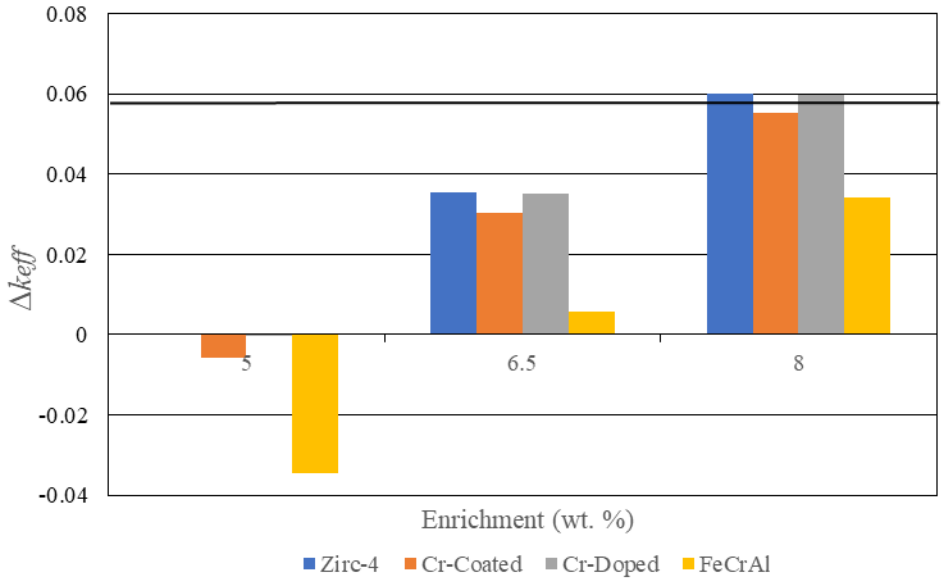

Figure 23. Changes from the baseline of the LEU+ and ATF changes for the PWR LD SFP DA model.

The results in Table 13 and

Table 14 show that the highest maximum k_{eff} calculated for the IA PWR SFP case is 0.9945 and the highest maximum k_{eff} calculated for the DA PWR SFP model is 1.0012, both occurring for the 8 wt % case with Zirc-4 cladding. For the IA PWR SFP, there are no cases that would result in an unacceptable reactivity increase with the current model; however, the DA PWR SFP model shows that it would be impossible to store an unshimmed 8 wt % fuel assembly without modifying the storage rack.

The results in Figure 22 and Figure 23 show the differential impacts of the LEU+ enrichment increases and ATF fuel forms. The impact of increasing the maximum enrichment from 5.0 to 6.5 wt % is ~0.039 Δk_{eff} for the IA rack and ~0.035 Δk_{eff} for the DA rack, and the impact of increasing the enrichment to 8.0 wt % is ~0.066 Δk_{eff} for the IA rack and ~0.060 Δk_{eff} for the DA rack. When examining the reactivity impacts of the ATF fuel and cladding forms, the Cr-coated cladding results in a reactivity decrease of ~0.005 Δk_{eff}, regardless of rack geometry or enrichment, and the Cr-doped fuel resulted in a reactivity decrease of less than 0.00050 Δk_{eff} for all cases. The FeCrAl fuel form results in a significant decrease in reactivity relative to the baseline model at the same enrichment. The FeCrAl reactivity decrease was approximately 0.031 at 5.0 wt % and 0.023 at 8.0 wt % for the IA rack and 0.035 Δk_{eff} at 5.0 wt % and 0.025 at 8.0 wt % for the DA rack.

3.2.1 Boron Degradation Response of IA SFP

To determine the effect of LEU+ enrichments on boron degradation, methods noted in Section 2.4.1 resulted in areal densities of the IA SFP poison paneling ranging from 0 (degraded) to 0.293 g/cm^2 (intact). Increments were taken in 10% steps with 2% sub steps in the final 10% to better express the removal of the absorber. Figure 24 plots the reactivity response with the increase in areal density from fully degraded to intact. For the 8.0 wt % case, 90% of the intact absorber (0.0264 g/cm^2) is required to maintain a maximum reactivity of 1.0. With 6.5 wt % fuel, 40% of the intact absorber (0.0117 g/cm^2) is required. The nominal enrichment requires 20% of the intact absorber (0.0059 g/cm^2). Figure 27 examines the final steps of degradation to visually enhance the deviation across LEU+ enrichments. The baseline in each curve is the intact absorber for the set enrichment. Upon full degradation, the use of 6.5 wt % fuel results in a 0.7 % Δk_{eff} increase over the Δk_{eff} observed with 5 wt %. The use of 8 wt % results in 1.2 % Δk_{eff} increase over the Δk_{eff} observed with 5 wt %. At 50% degradation (0.0147 g/cm^2) 6.5 wt % results in a 0.1 % Δk_{eff} increase over the 5 wt % Δk_{eff}, and 6.5 wt % results in a 0.2 % Δk_{eff} increase over the 5 wt % Δk_{eff}. Increased degradation with LEU+ enrichments results in a heightened relative increase in k_{eff}.

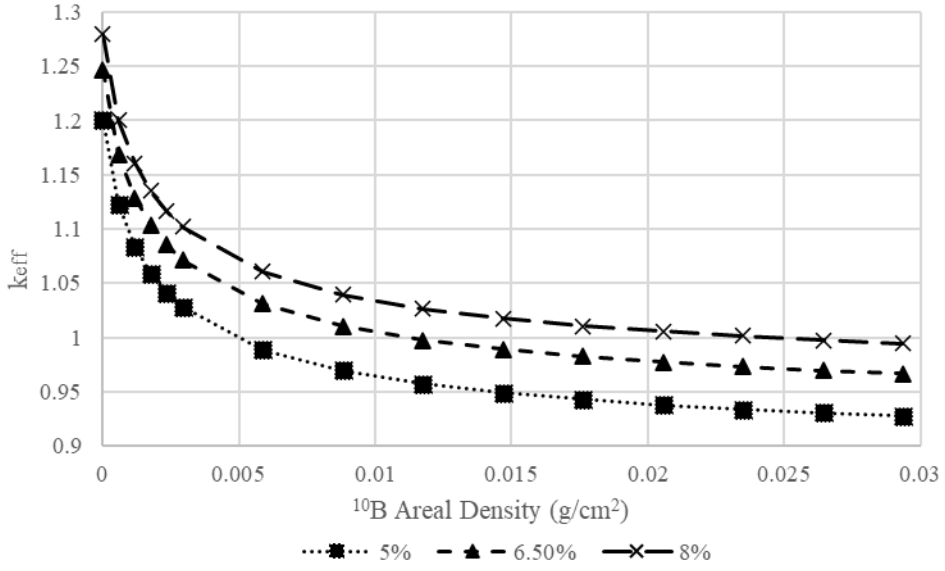

Figure 24. IA SFP poison panel degradation

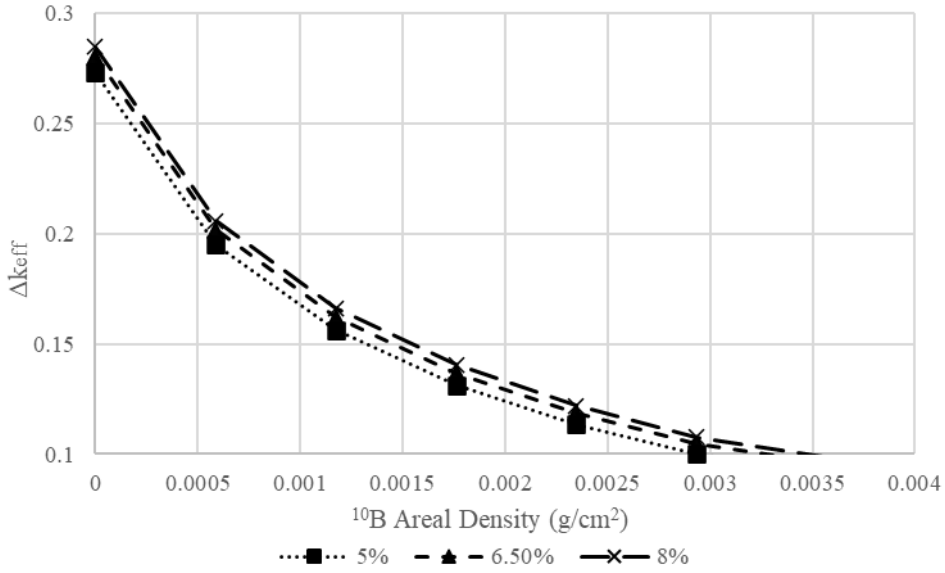

Figure 25. IA SFP poison panel degradation relative to fully intact

3.3 SOLUBLE BORON CONCENTRATION AND MISLOAD EVALUATION

This section provides the results of the SBC evaluation for normal and accident conditions following the methods discussed in Section 2.4.2.

To investigate the amount of SBC needed to meet the 0.95 k_{eff} limit under normal conditions, soluble boron was added to the SFP models in increments of 100 ppm ranging from 0 to 2,000 ppmB. The results of the SBC calculations for IA normal operations are shown in Figure 26, with results for the DA in Figure 27.

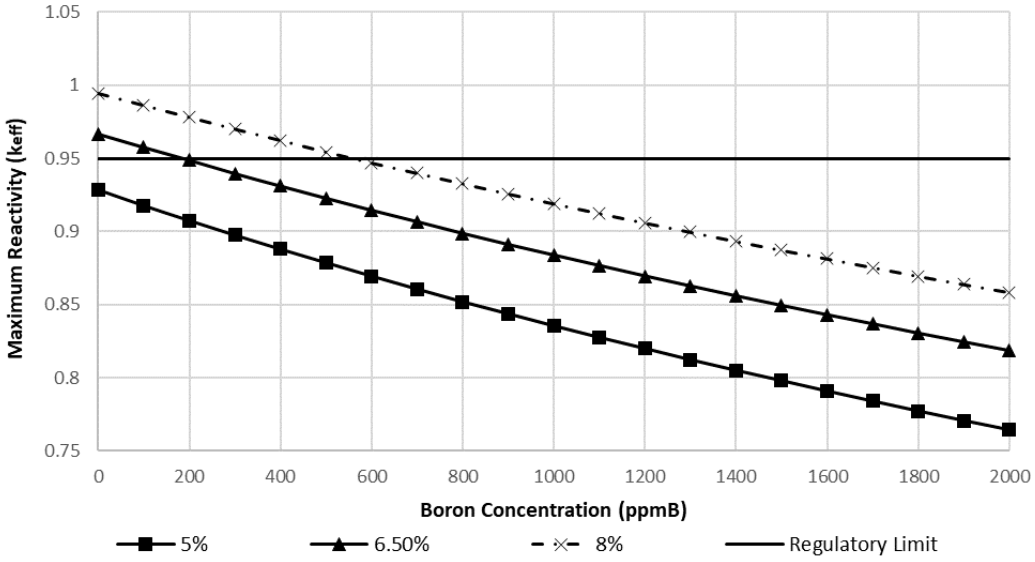

Figure 26. Normal condition PWR IA SFP boron worth by fuel loading.

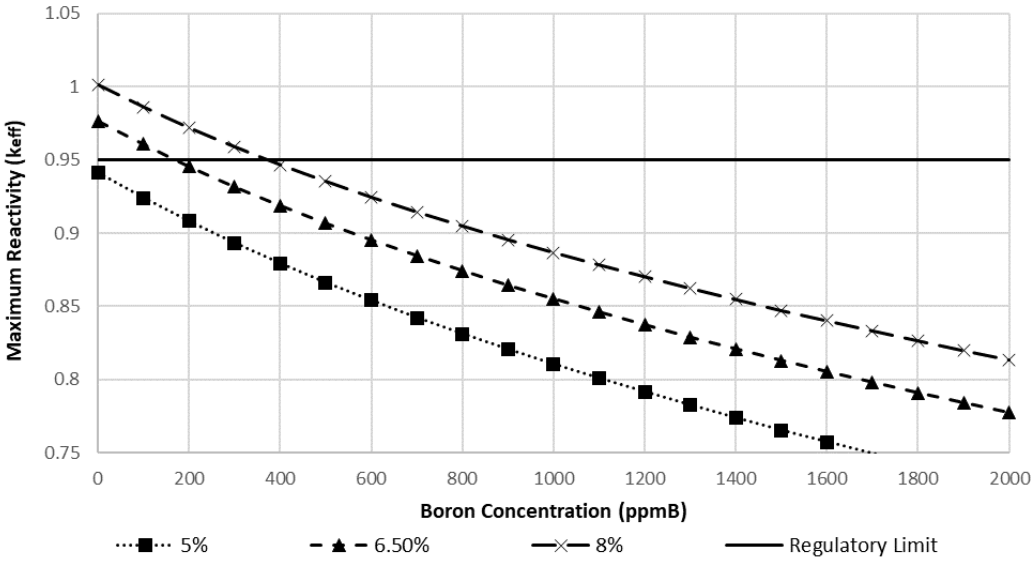

Figure 27. Normal condition PWR DA SFP boron worth by fuel loading

For the 8.0 wt % IA unshimmed case, as the most reactive configuration, 600 ppmB is required to maintain a maximum reactivity of 0.95. With 6.5% fuel, 200 ppmB is required. For the 8.0 wt % DA unshimmed case, 400 ppmB is required to maintain a maximum reactivity of 0.95. With 6.5% fuel, 200 ppmB is required. Following the misload pattern for the SFP DA model shown in Figure 9, misload calculations were performed, and the results are plotted in Figure 28 as a function of the number of misloaded assemblies.

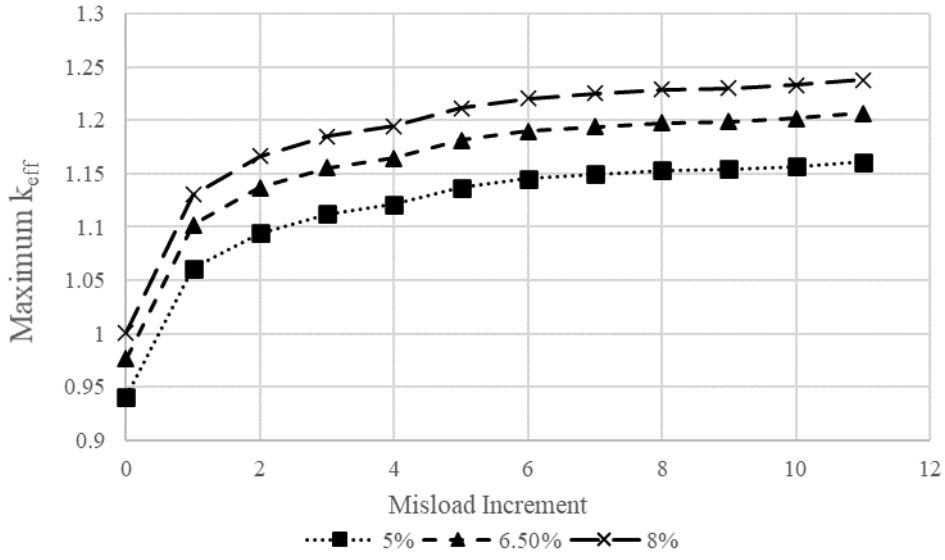

Figure 28. DA SFP maximum k_{eff} as a function of the number of misloaded assemblies.

The single misload presents the largest k_{eff} increase by any single assembly misload, representing ~55% of the total reactivity increase for each enrichment. To offset the increase in reactivity from the misload, borated water was credited to determine the necessary concentration to offset the accident. This produced

the following boron worth curves with the misloading of one, five, and 11 unshimmed assemblies in Figure 29, Figure 30, and Figure 31.

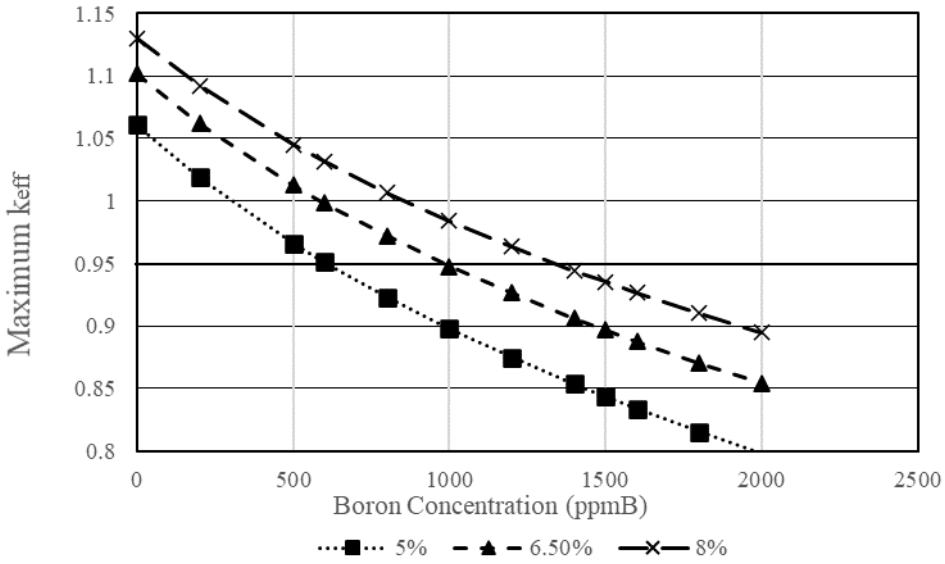

Figure 29. Boron worth for one misloaded assembly.

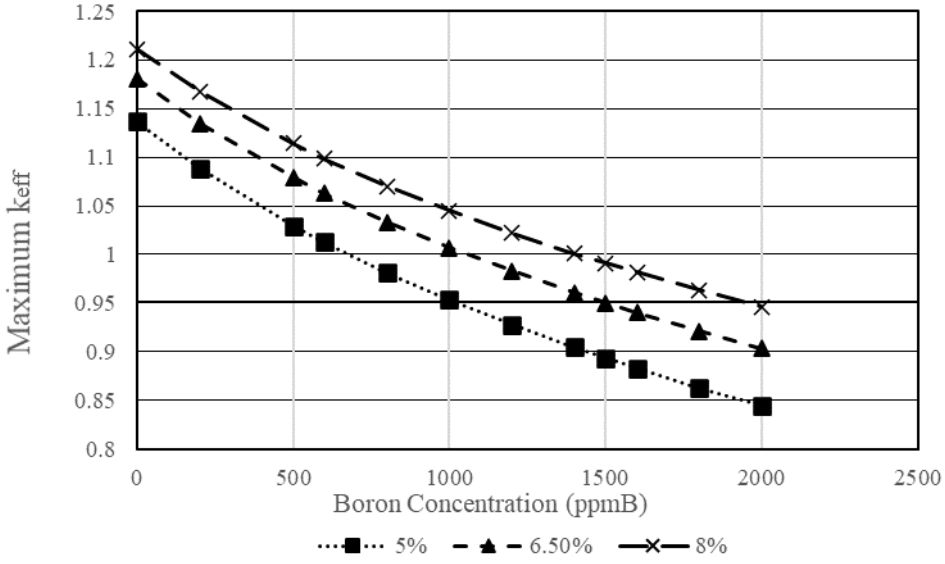

Figure 30. Boron worth for five misloaded assemblies.

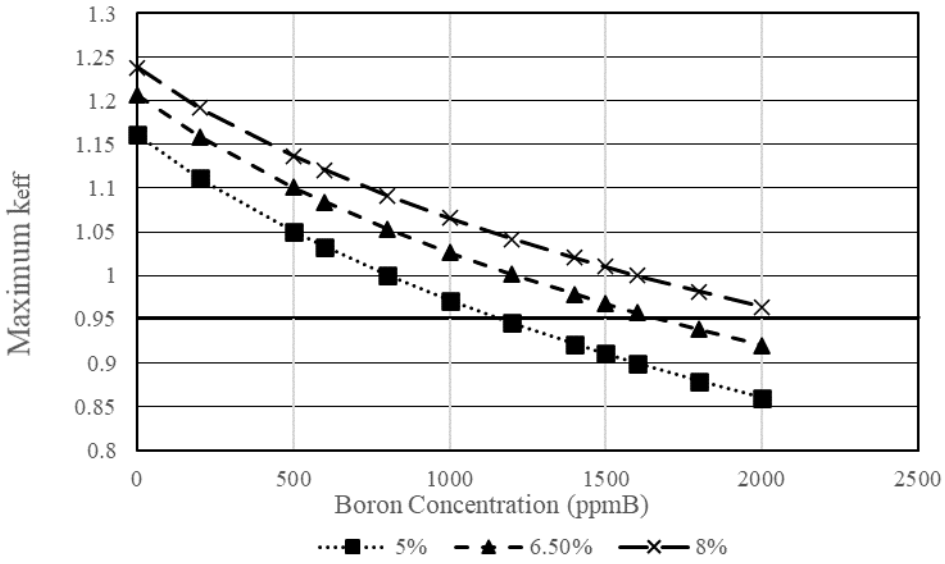

Figure 31. Boron worth for 11 misloaded assemblies.

In the baseline 5 wt % case, one misload requires approximately 600 ppmB to maintain the 0.95 limit of subcriticality. The 6.5 wt % case fuel requires 1,000 ppmB for a maximum k_{eff} of 0.95. The highest enrichment in this study at 8.0 wt % requires 1,400 ppmB. No credit for burnable absorbers is used here. For the single assembly misload case in the DA SFP rack model, each 1.5% increase in enrichment corresponded to an approximate additional 400 ppmB needed to meet the 0.95 subcritical limit.

In the baseline case, five misloaded assemblies require approximately 1,000 ppmB to maintain the 0.95 limit of subcriticality. The 6.5 wt % case requires 1,500 ppmB to keep the maximum k_{eff} less than 0.95. The 8.0 wt % case requires 2,000 ppmB. Unshimmed for five assembly misloads, each 1.5% increase in enrichment corresponded to an approximate additional 500 ppmB for the 0.95 limit.

The baseline 11 misloaded assemblies case requires approximately 1,200 ppmB to maintain the 0.95 limit of subcriticality. Using 6.5% enriched unshimmed fuel requires 1,600 ppmB for a maximum k_{eff} of 0.95. The highest enrichment in this study at the 8 wt % case requires more than 2,000 ppmB. Unshimmed for 11 assembly misloads, each 1.5% increase in enrichment corresponded to an approximate additional 450 ppmB for the 0.95 limit.

3.4 BWR NFV

3.4.1 Fully Flooded

This section discusses the results of the fully flooded BWR NFV sensitivity study for LEU+ and ATF fuel forms. The fully flooded condition is modeled by filling the entire BWR NFV model with nominal density water. Table 15 displays the results for the baseline 4.7 wt % enriched case, as well as the results for the 6.5 and 8.0 wt % enriched LEU+ cases. Results are presented for the Zirc-2 clad fuel, as well as the Cr-coated, Cr-doped, and FeCrAl ATF fuel rod designs. The standard Zirc-2 cladding and UO_2 fuel is the limiting condition for the BWR NFV. For each case, a sum of biases and uncertainties was assumed to be 0.03 Δk_{eff}. The maximum k_{eff} values are calculated by adding the sum of biases and uncertainties to the calculated k_{eff} and are reported in Table 15. Figure 32 plots these values relative to the nominal Zirc-2 4.7% case, and the regulatory limit of 0.95 is indicated by the black bar.

Table 15. Fully flooded BWR NFV k_{eff}.

	ATF cladding material			
Fuel enrichment (wt %)	**Zirc-2**	**Cr-coated**	**Cr-doped**	**FeCrAl**
4.7	0.9451	0.9416	0.9443	0.9252
6.5	1.0209	1.0177	1.0205	1.0035
8.0	1.0651	1.0623	1.0645	1.0490

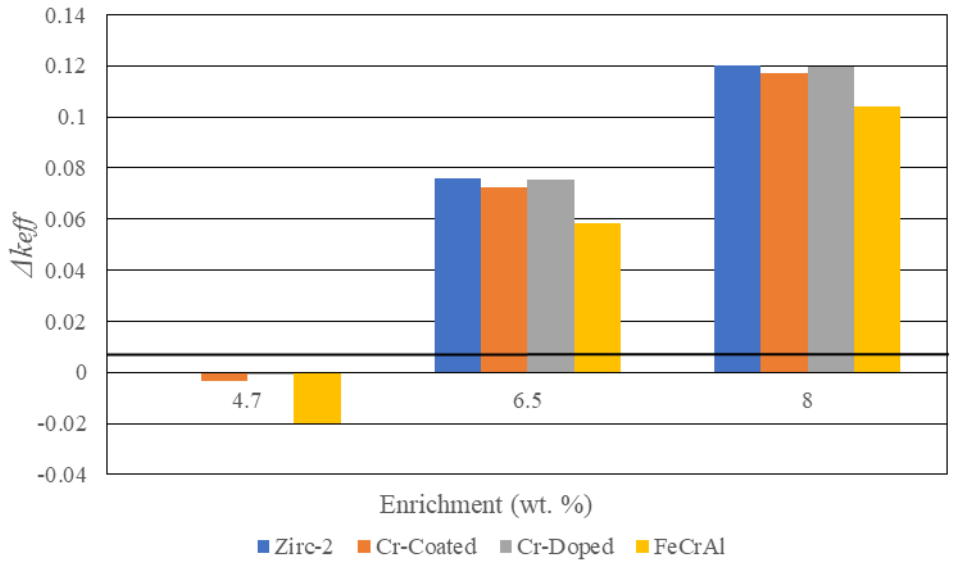

Figure 32. Changes from the baseline of the LEU+ and ATF changes for the fully flooded BWR NFV model.

The results in Table 15 show that all the 6.5 and 8.0 wt % cases result in supercritical configurations, regardless of the ATF fuel form configuration. It would be impossible to store fuel of this enrichment without additional credit for absorber material or restricting the loading of the NFV. This is further explored in Section 3.5. The differential changes of LEU+ and ATF fuel forms from the baseline are shown in Figure 32. The results in Figure 32 show that the increase from 4.7 to 6.5 wt % results in a ~0.078 Δk_{eff} increase, and the increase from 4.7 to 8.0 wt % results in an increase of ~0.12 Δk_{eff}. The impact of the Cr-coated cladding is ~0.003 Δk_{eff}, and the impact of the Cr-doped fuel form is negligible, regardless of enrichment. The FeCrAl shows a significant suppressive effect that is enrichment dependent. The effect of the FeCrAl fuel form is ~0.020 Δk_{eff} for the 4.7 wt % case and ~0.016 Δk_{eff} for the 8 wt % case.

BWR enrichment increases in k_{eff} are nearly double those observed with PWR enrichment increases, with PWR vaults and SFPs increasing on the order of 6% k_{eff} compared to the 12% observed with the BWR vault. BWR fuel rods are thicker than PWR rods, and BWRs typically have much more variable enrichment loading schemes axially and radially. In practice, as evidenced in Cumberland et al. [14], a core average enrichment of 6.5% relates more to a true BWR core of 8.5% maximum enrichment, and a core average enrichment of 7.4% correlates to a 10% maximum enrichment. The fuel enrichments in the modeled PWR and BWR assemblies are implemented identically with uniform enrichments of 6.5 and 8% across the assembly, not accounting for the differences in actual operation, and result in significantly higher k_{eff} values for the BWR cases.

3.5 ABSORBER CREDIT TO OFFSET INCREASED ENRICHMENT

The baseline UO_2 fuel with zircaloy cladding is the most reactive fuel type for criticality in all fully flooded models. For variable density moderation in the PWR NFV, the use of Cr-Doped fuel results in small increases in k_{eff} at several densities, although the magnitude is on the order of Monte Carlo uncertainty and at the non-optimum conditions. Therefore, the Zirc-4 clad UO_2 fuel was also considered the limiting condition for optimum moderation of the PWR NFV (referred to as "Standard"). To account for uncertainties in the SFP and NFV, model dimensions and compositions margins of 0.02 for the PWR calculations and 0.03 for the BWR were assumed and added to the best estimate k_{eff} values to determine the maximum k_{eff} values. A summary of the LEU+ maximum k_{eff} values obtained in the previous sections is provided in Table 16.

Table 16. Limiting k_{eff} of ATF variants.

Storage Array	PWR NFV		PWR IA SFP		PWR DA SFP		BWR NFV	
Enrichment	6.5%	8%	6.5%	8%	6.5%	8%	6.5%	8%
Limiting ATF condition	Standard	Standard	Standard	Standard	Standard	Standard	Standard	Standard
Fully flooded	0.9767	1.0003	0.9667	0.9945	0.9766	1.0012	1.0209	1.0651
Optimum moderation	0.9502	0.9798						

To satisfy the regulatory limits, NFVs must show that the maximum k_{eff} values are less than 0.95 under fully flooded conditions and less than 0.98 under optimum moderation conditions, and PWR SFP must show that the maximum k_{eff} is less than 1.0 with no SBC and less than 0.95 with SBC. Table 16 indicates that additional reactivity credit is necessary for nearly all the fully flooded configurations with some level of LEU+ fuel.

Most fuel assemblies used with LEU enrichments have some degree of integral burnable absorber, so it is reasonable to assume that the LEU+ fuel will incorporate burnable absorbers. Gadolinia is universally employed in BWR fuel assemblies, and either gadolinia or IFBA are typically used for PWR fuel, so these types of absorbers were investigated as a means of demonstrating the subcriticality of LEU+ fuel in the configurations investigated.

Incorporating 12 gadolinia rods with at least 2 wt % Gd_2O_3 is common in modern BWR fuel management. In Cumberland et al. [14], the authors investigated the reactor physics operation of LEU+ and burnup in BWRs, and their report used 16 and 20 gadolinia rods, which proved to be sufficient, if not desired, from a reactor physics perspective. Given this information, ranges of gadolinia rods from 12 to 20 were considered. Additionally, increased gadolinia loadings of up to 4 wt % were also analyzed. For PWR arrays, a thin layer of ZrB_2 was deposited onto specific fuel rods to represent IFBA. The use of 32, 64, and 80 IFBA rods was investigated. The IFBA loading used in the analysis is 2.35 mg ^{10}B/in. The removal of assemblies from their storage cell was also investigated apart from the PWR DA SFP, which originally had two empty cells. Figure 33 and Figure 34 show the gadolinia and IFBA patterns used.

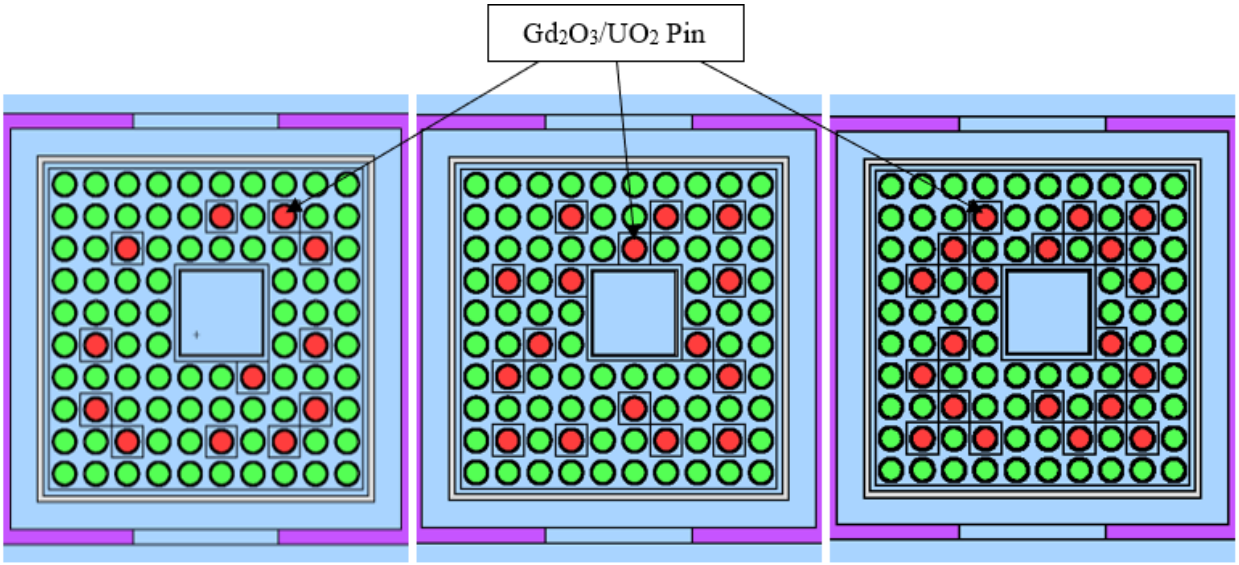

Figure 33. Twelve, 16, and 20 rod gadolinia layout for BWR.

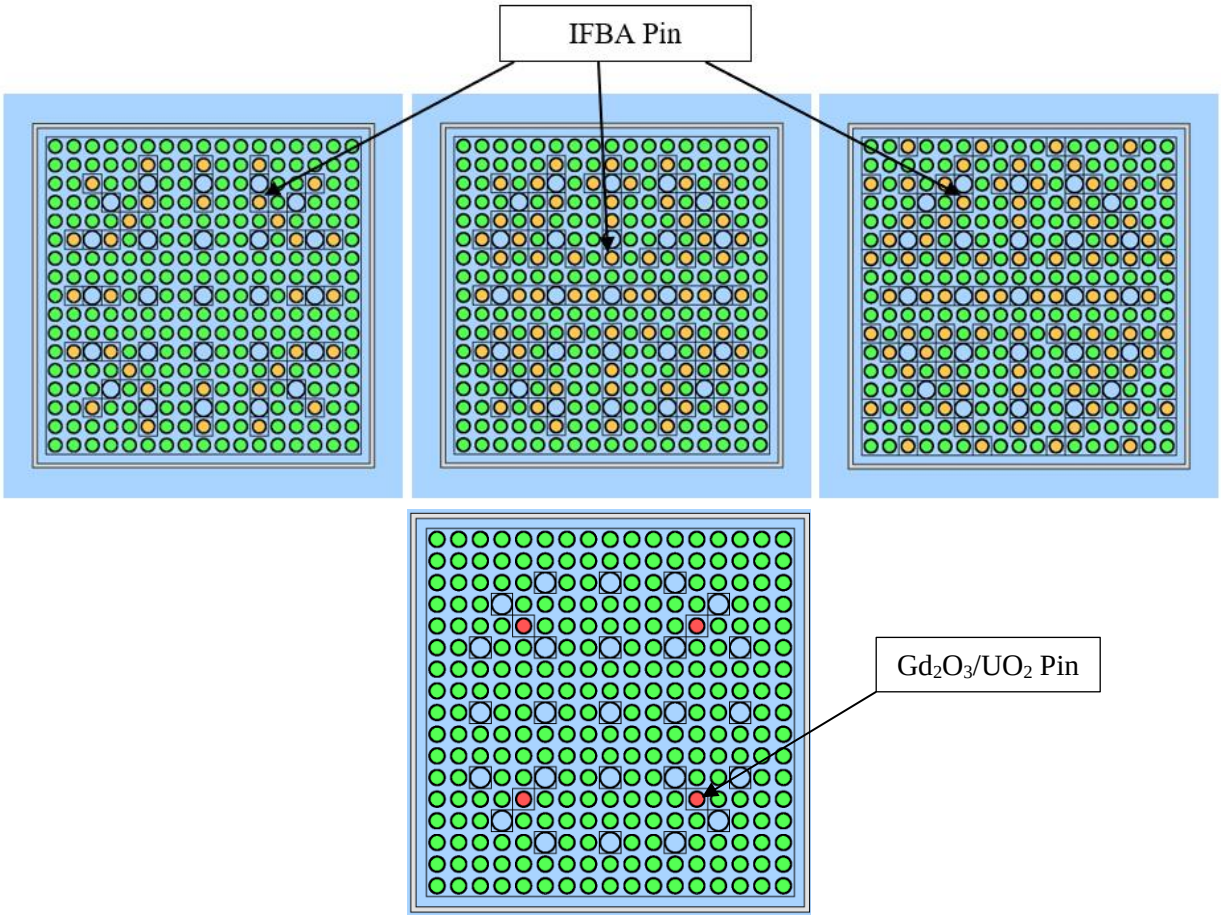

Figure 34. Thirty-two, 64, and 80 IFBA and four gadolinia rod layout for PWR(not to scale).

Additionally, the effect of removing assemblies from cells was investigated for models, excluding the DA SFP with originally two empty cells. The IA SFP removed one assembly from the 2 × 2 cell array, or a

75% loading. The PWR NFV with two arrays of 7 × 5 cells had six central cornered assemblies removed because one in every four could not be removed with 35 assemblies per array. The PWR NFV assembly removal resulted in 83% loading. The BWR NFV removed every fourth element in the array of 21 × 10 rack cells. The non-divisible length of cells left an extra row of fully filled assemblies, resulting in 76% loading. These configurations are shown in Figure 35.

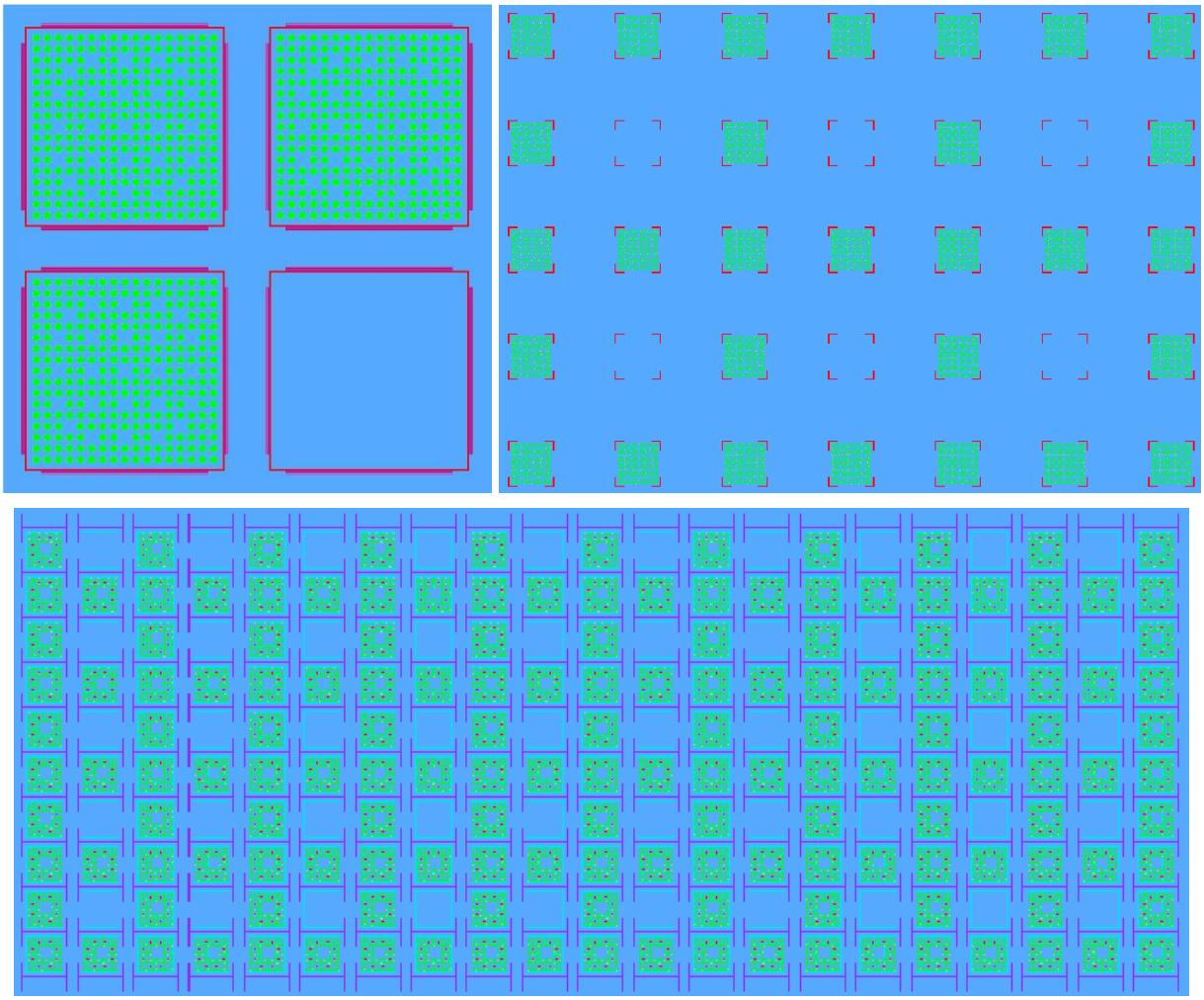

Figure 35. Array loading schemes for assembly removal. Clockwise from the top left: PWR IA SFP, PWR NFV, and BWR NFV.

Table 17 through Table 20 present the k_{eff} values and the reactivity change for 6.5 and 8 wt % UO_2 for each storage array and burnable absorber combination. All cases were found to be sufficiently mitigated with reasonable burnable absorber requirements being imposed. Actual burnable absorbers implemented and loaded are determined by the operator. For example, the BWR NFV with 6.5% enriched fuel is sufficiently subcritical with 16 gadolinia rods—perhaps overly so for storage and reactor physics purposes. Operators may instead opt for 14 rods, an option that was not investigated but is likely to be sufficiently subcritical based on the trend in increasing gadolinia rods; alternatively, 12 rods at 6% gadolinia may be sufficient, for example.

Table 17. BWR NFV reactivity credits.

Configuration	Array loading (%)	Gd wt %	Gd rods	Absorber Δk_{eff}		Maximum reactivity (k_{eff})	
				6.5%	8%	6.5% k_{eff}	8% k_{eff}
Base	100	2	8	0	0	1.0209	1.0651
+1% Gd	100	3	8	-0.0058	-0.0059	1.0151	1.0592
+2% Gd	100	4	8	-0.0099	-0.0099	1.0110	1.0552
+4 rods	100	2	12	-0.0455	-0.0415	0.9754	1.0236
+1% Gd, +4 rods	100	3	12	-0.0539	-0.0499	0.9670	1.0152
+2% Gd, +4 rods	100	4	12	-0.0595	-0.0556	0.9614	1.0095
+8 rods	100	2	16	-0.0997	-0.0922	0.9212	0.9729
+1% Gd, +8 rods	100	3	16	-0.1106	-0.1030	0.9103	0.9621
+2% Gd, +8 rods	100	4	16	-0.1181	-0.1109	0.9028	0.9542
+12 rods	100	2	20	-0.1318	-0.1218	0.8891	0.9433
+1% Gd, +12 rods	100	3	20	-0.1440	-0.1343	0.8769	0.9308
+2% Gd, +12 rods	100	4	20	-0.1526	-0.1429	0.8683	0.9222
-1 assembly	76	2	8	-0.1166	-0.1216	0.9043	0.9435
-1 assembly, +1% Gd	76	3	8	-0.1221	-0.1269	0.8988	0.9382
-1 assembly, +2% Gd	76	4	8	-0.1256	-0.1305	0.8953	0.9346

Table 18. PWR NFV reactivity credits.

Configuration	Array loading (%)	Gd wt %	Gd rods	IFBA rods	Absorber Δk_{eff}		Maximum reactivity (k_{eff})	
					6.5% k_{eff}	8% k_{eff}		
Base	100	0	0	0	0.0000	0.0000	0.9767	1.0003
+32 rods	100	0	0	32	-0.0330	-0.0290	0.9437	0.9713
+64 rods	100	0	0	64	-0.0720	-0.0637	0.9047	0.9366
-1 assembly	83	0	0	0	-0.0003	-0.0003	0.9764	1.0000
-1 assembly, +32 rods	83	0	0	32	-0.0335	-0.0295	0.9432	0.9708
-1 assembly, +64 rods	83	0	0	64	-0.0724	-0.0641	0.9043	0.9362
+4 Gd rods (2%)	100	2	4	0	-0.0195	-0.0174	0.9572	0.9829
+4 Gd rods (3%)	100	3	4	0	-0.0207	-0.0187	0.9560	0.9816
+4 Gd rods (4%)	100	4	4	0	-0.0218	-0.0196	0.9549	0.9807

Table 19. PWR IA SFP hardware modifications.

Configuration	Array loading (%)	Gd wt %	Gd rods	IFBA rods	Absorber Δk_{eff}		Maximum reactivity (k_{eff})	
					6.5%	8%		
Base	100	0	0	0	0	0	0.9667	0.9945
+32 rods	100	0	0	32	-0.0335	-0.0298	0.9332	0.9647
+64 rods	100	0	0	64	-0.0763	-0.0676	0.8904	0.9269
-1 assembly	75	0	0	0	-0.0418	-0.0434	0.9249	0.9511
-1 assembly, +32 rods	75	0	0	32	-0.0733	-0.0715	0.8934	0.9230
-1 assembly, +64 rods	75	0	0	64	-0.1153	-0.1086	0.8514	0.8859
+4 Gd rods (2%)	100	2	4	0	-0.0220	-0.0192	0.9447	0.9753
+4 Gd rods (3%)	100	3	4	0	-0.0232	-0.0209	0.9435	0.9736
+4 Gd rods (4%)	100	4	4	0	-0.0243	-0.0219	0.9424	0.9726

Table 20. PWR DA SFP hardware modifications.

Configuration	Array loading (%)	Gd wt %	Gd rods	IFBA rods	Absorber Δk_{eff}		Maximum reactivity (k_{eff})	
					6.5%	8%		
Base	50	0	0	0	0	0	0.9766	1.0012
+32 rods	50	0	0	32	-0.0330	-0.0290	0.9436	0.9722
+64 rods	50	0	0	64	-0.0717	-0.0638	0.9049	0.9374
+80 rods	50	0	0	80	-0.0847	-0.0756	0.8919	0.9256
+4 Gd rods (2%)	50	2	4	0	-0.0198	-0.0175	0.9568	0.9837
+4 Gd rods (3%)	50	3	4	0	-0.0211	-0.0187	0.9555	0.9825
+4 Gd rods (4%)	50	4	4	0	-0.0221	-0.0198	0.9545	0.9814

Removing every fourth assembly significantly affected the BWR NFV with a maximum reactivity in the 8% case on par with crediting 20 gadolinia rods. The PWR NFV has no meaningful variation in k_{eff} as a result of removing assemblies. Thirty-two and 64 credited IFBA rods satisfy regulatory limits for both 6.5 and 8% enrichment. Although four gadolinia rods are insufficient in either case, at 6.5%, an additional rod or an increased Gd loading would likely reduce k_{eff} below 0.95. Eight percent enrichment would likely require a further eight gadolinia rods.

Both PWR SFPs are satisfactorily below a maximum reactivity of 1.0 in their base configuration at 6.5% enrichments. Mitigation techniques were investigated to ensure acceptable margin at little computational expense. The DA case at 8% is slightly above the limit of 1.0, and all examined mitigation techniques were successful in reducing reactivity below the regulatory limit.

Although it was an option examined for all models other than the DA SFP, removing assemblies was considered secondary to crediting integral burnable absorbers. Table 21 provides the configurations chosen to meet regulatory limits, as well as the maximum reactivity continuous energy calculations. The bias of the multigroup results are less than 150 pcm in PWR cases and less than 250 pcm in the BWR NFV cases. The biases range from -0.0023 to 0.0014 Δk.

Table 21. Final configuration maximum reactivities.

Storage array	PWR NFV		PWR IA SFP		PWR DA SFP		BWR NFV	
Enrichment	**6.5%**	**8%**	**6.5%**	**8%**	**6.5%**	**8%**	**6.5%**	**8%**
Burnable absorber	32 IFBA	64 IFBA	Base	Base	Base	32 IFBA	16 Gd, 2 wt %	20 Gd, 2 wt %
Multigroup	0.9437	0.9366	0.9667	0.9945	0.9766	0.9722	0.9212	0.9433
Continuous energy	0.9439	0.9372	0.9674	0.9954	0.9779	0.9736	0.9189	0.9420

Although the optimum moderation condition remains under 0.98 without crediting the absorber, Table 22 presents the final configuration of the PWR NFV to confirm that additional absorber credit does not unexpectedly increase optimum moderation maximum reactivity. Maximum reactivities remain well below 0.98 at all densities.

Table 22. Absorber credited PWR NFV optimum moderation maximum reactivities.

Moderator density (%)	32 IFBA 6.5%	64 IFBA 8%
1	0.5767	0.5999
5	0.8885	0.9088
6	0.9121	0.9321
7	0.9225	0.9430
8	0.9238	0.9444
9	0.9181	0.9388
10	0.9078	0.9284
20	0.7385	0.7561
30	0.6571	0.6706
40	0.6615	0.6708
50	0.7021	0.7082
60	0.7539	0.7567
70	0.8062	0.8063
80	0.8561	0.8537
90	0.9019	0.8971
100	0.9437	0.9366

Figure 36 plots the k_{eff} differential relative to the fully flooded condition for each noted configuration. The unshimmed 5, 6.5, and 8% enrichment differentials are on par with one another, whereas introducing IFBA leads to smaller k_{eff} differences. With 64 IFBA rods, the optimum moderation k_{eff} is higher than fully flooded. Both conditions meet the regulatory limits, but it is apparent that adding further IFBA rods to counter higher enrichments could meet the optimum moderation limit, whereas the fully flooded would not.

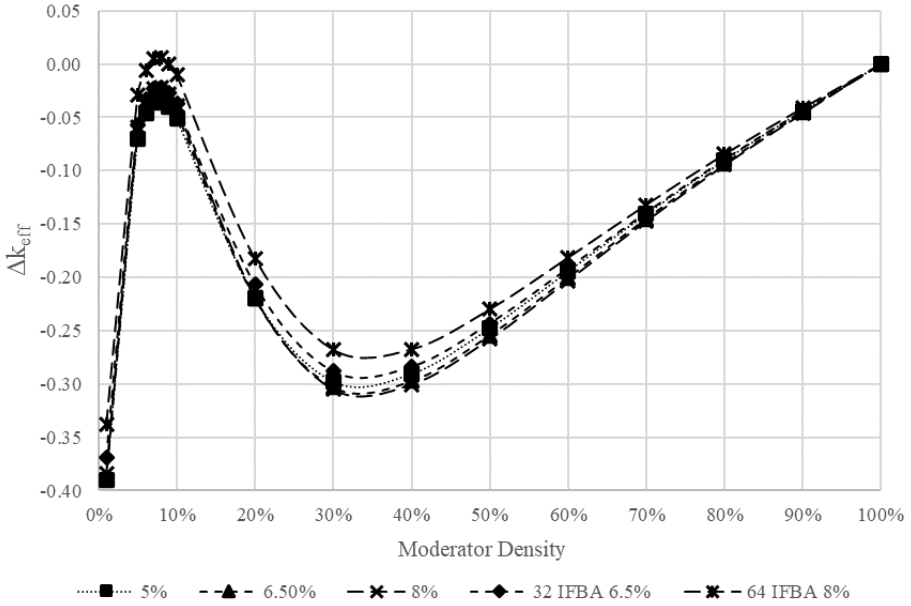

Figure 36. PWR NFV mitigation Δk_{eff} relative to fully flooded.

Figure 37 plots the relative variation in k_{eff} with the nominal enrichment as a function of moderator density as the baseline. This exhibits that the increased enrichment does not result in a flat increase in k_{eff} at all densities, nor should that be expected. Again, with increased enrichment and IFBA, the lower moderation results in higher k_{eff}, despite 6.5% with 32 rods on par with 5% fully flooded and 8% with 64 rods being below 5% fully flooded.

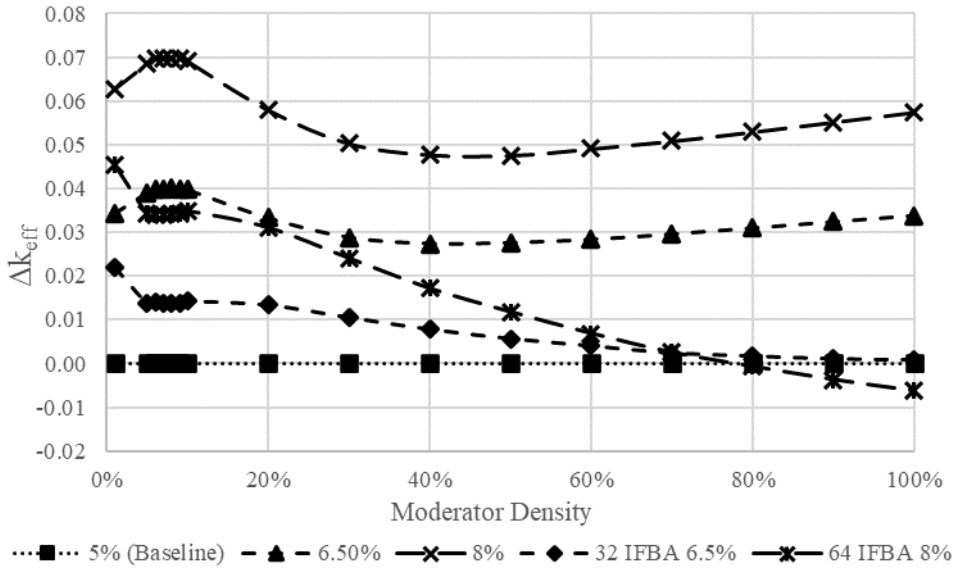

Figure 37. PWR NFV with and without mitigation relative to 5%.

3.6 IMPACT OF ENRICHMENT CHANGES ON MODELING CONSIDERATIONS

3.6.1 Neutronic Decoupling Distance Evaluation

The neutronic decoupling distance was evaluated by using the methods discussed in Section 2.6.1 for the W 17 × 17 STD PWR fuel design and the ATRIUM 10 BWR fuel design. A series of calculations was run with a range of edge-to-edge separations to determine the difference in the k_{eff} values between the maximally separated and each of the shorter distances. The Δk_{eff} results of these calculations are plotted in Figure 38Figure 26 for the W 17 × 17 STD (left) and ATRIUM 10 (right) assembly designs.

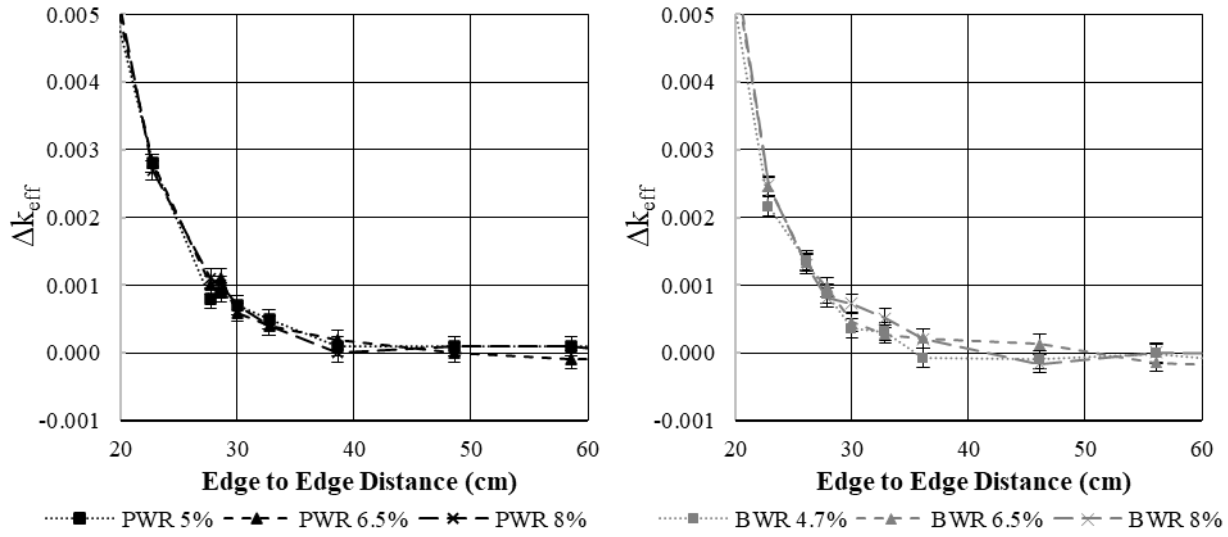

Figure 38. PWR and BWR criticality differential with assembly spacing.

The results in Figure 38 demonstrate the indistinguishability between enrichments regarding the separation distance between two assemblies for both PWR and BWR fuel. Although the exact point of decoupling may be debated, nominal enrichment assemblies at 30 cm have less than 0.00075 difference in k_{eff} from the maximum separation, as do LEU+ assemblies.

3.6.2 Eccentric Positioning Evaluation

Using the eccentric positioning configurations discussed in Section 2.6.2, the eccentric positioning bias was calculated for each of the storage configurations considered. The eccentric positioning biases are shown in Table 23 for the fully flooded PWR NFV, Table 24 for the BWR NFV, Table 25 for the IA PWR SFP model, and Table 26 the DA PWR SFP model. Data are expressed as Δk_{eff}, calculated as the nominal configuration k_{eff} subtracted from the eccentric positioned k_{eff}.

Table 23. PWR NFV eccentric positioning effect.

	Fuel enrichment (wt %)	Nominal	Eccentric	Δk_{eff}
Fully Flooded	5.0	0.9229	0.9231	0.0002
	6.5	0.9567	0.9572	0.0005
	8.0	0.9803	0.9806	0.0003
Optimum Moderation	5.0	0.8901	0.8924	0.0023
	6.5	0.9302	0.9324	0.0022
	8.0	0.9598	0.9623	0.0025

Table 24. BWR NFV eccentric positioning effect.

Fuel enrichment (wt %)	Nominal	Eccentric	Δk_{eff}
4.7	0.9151	0.9351	0.0200
6.5	0.9909	1.0132	0.0223
8.0	1.0351	1.0586	0.0235

Table 25. PWR IA SFP eccentric positioning effect.

Fuel enrichment (wt %)	Nominal	Eccentric	Δk_{eff}
5.0	0.9078	0.9070	-0.0008
6.5	0.9467	0.9464	-0.0003
8.0	0.9745	0.9745	0.0000

Table 26. PWR DA SFP eccentric positioning effect.

Fuel enrichment (wt %)	Nominal	Eccentric	Δk_{eff}
5.0	0.9212	0.9231	0.0019
6.5	0.9566	0.9585	0.0019
8.0	0.9812	0.9836	0.0024

PWR model eccentricity effects show less than 50 pcm differences between enrichments. Optimum moderation NFV is more sensitive to eccentricities. The effect of eccentric positioning is below 0.25% Δk_{eff} for all PWR configurations. Eccentric positioning in the BWR model produces 2% Δk_{eff} with the effect increasing 0.35% Δk_{eff} between an enrichment of 4.7 and 8%.

3.6.3 Radial Enrichment Averaging in BWRs

Using the minimum critical configurations noted in Section 2.7, the following data were produced for the GE 14 assemblies with given enrichment zoning and the average. The Δk_{eff} is expressed as the pin-wise enrichment k_{eff} subtracted from the lattice averaged enrichment. Table 27 shows the impact of BWR assembly enrichment averaging.

Table 28. BWR assembly enrichment averaging.

Fuel enrichment (average wt %)	Pin-wise	Lattice averaged	Δk_{eff}
4.3	0.7492	0.7551	0.0059
6.5	0.8596	0.8638	0.0042
8.0	0.9117	0.9151	0.0034

Although the effect of lattice averaging the enrichment remains positive for all cases considered, the effect decreases in magnitude as a function of increasing enrichment.

3.6.4 Assembly Clustering Evaluation

Calculations were performed for the assembly clustering configurations shown in Figure 15 for BWR fuel and Figure 16 for PWR fuel using the methods described in Section 2.8. The following data were produced for the W 17 × 17 STD and Atrium 10 assemblies. The results of the assembly clustering analysis are shown in Figure 39 from the ATRIUM 10 assembly and in Figure 40 for the unshimmed W 17 × 17 STD assembly.

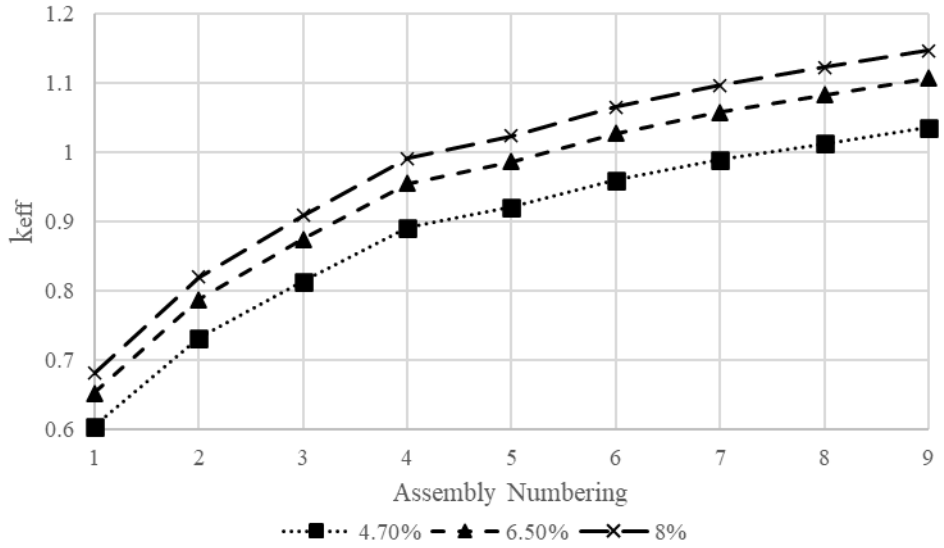

Figure 39. k_{eff} as a function of clustered BWR assemblies.

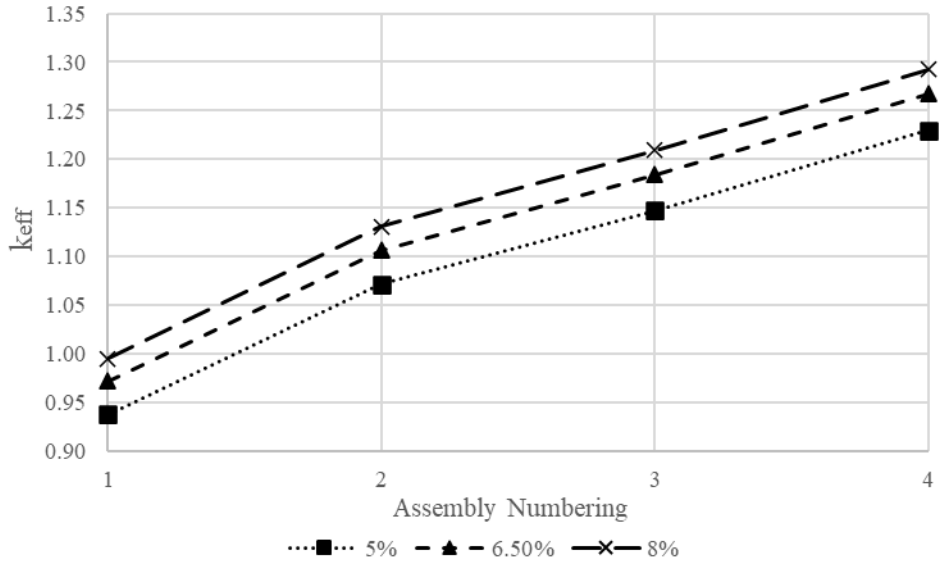

Figure 40. k_{eff} as a function of clustered PWR assemblies, unshimmed.

The results in Figure 39 for BWR assemblies with the baseline 5 wt % enrichment require eight clustered assemblies to get to a calculated k_{eff} of ~1, whereas the increased enrichments at 6.5 and 8 wt % require five and four clustered assemblies, respectively. The results in Figure 40 show for the baseline 5.0 wt % case that two unshimmed assemblies are sufficient to obtain criticality in unborated water, and the LEU+ cases result in an increase in reactivity above that. For the case of one unshimmed assembly, the 8.0 wt % case has a k_{eff} of ~0.995. It is expected to be unlikely for assemblies of this enrichment to have no integral absorber. To determine what the results would be in the presence of an integral absorber, additional calculations were repeated with 32 and 64 IFBA rods. The results of the assembly clustering analysis are shown in Figure 41 for the 32 IFBA case and in Figure 42 for the 64 IFBA case.

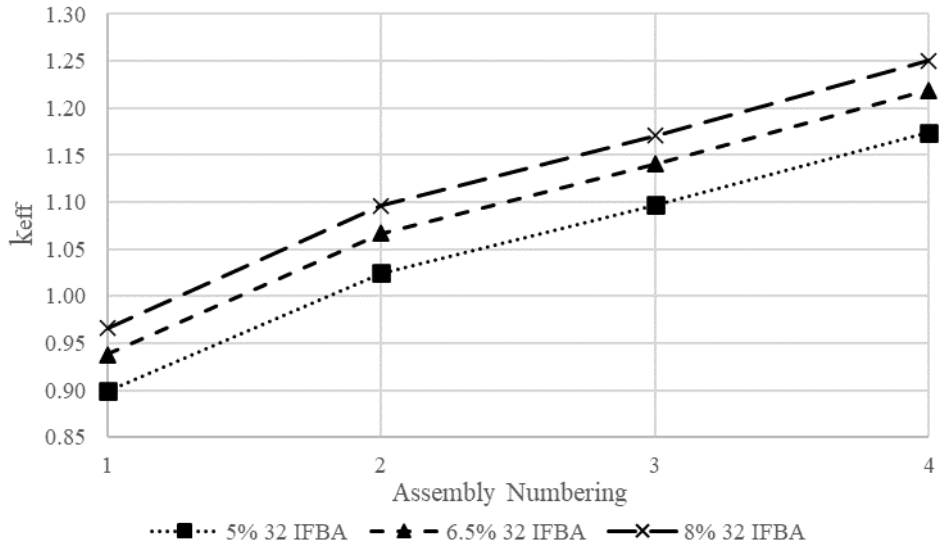

Figure 41. k_{eff} as a function of clustered PWR assemblies for 32 IFBA.

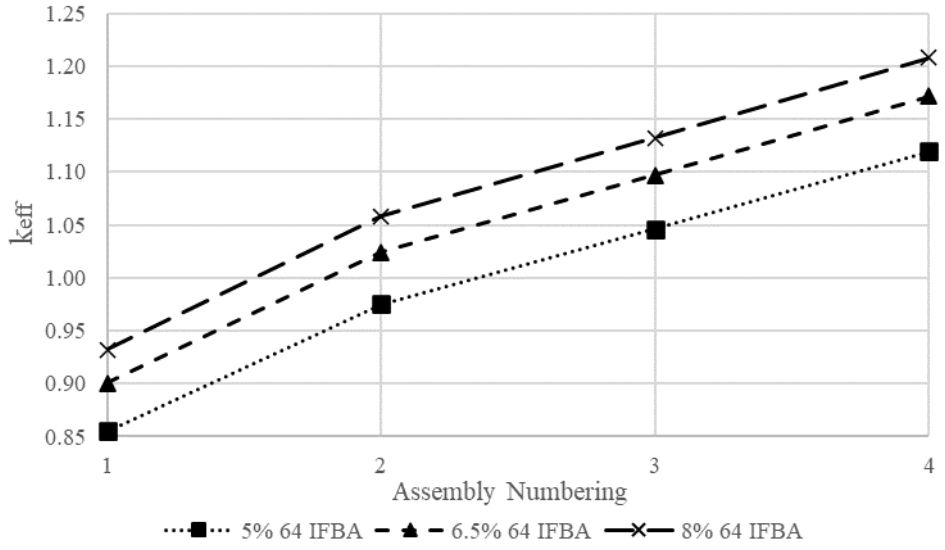

Figure 42. k_{eff} as a function of clustered PWR assemblies for 64 IFBA.

The results of the assembly clustering calculations with IFBA credit show reductions in reactivity but do not meaningfully change the number of assemblies required for criticality for the LEU+ cases. Including 32 IFBA rods reduces the reactivity of the single assembly case by 0.039 Δk_{eff} for the 5 wt % case and 0.029 Δk_{eff} for the 8 wt % case. Including 64 IFBA rods reduces the reactivity 0.083 Δk_{eff} for the 5 wt % case and 0.063 Δk_{eff} for the 8 wt % case. If two assemblies are in close contact, then including 32 IFBA rods decreases the reactivity by 0.046 Δk_{eff} for the 5 wt % case and reduces the reactivity by 0.035 Δk_{eff} for the 8 wt % case and including 64 IFBA rods reduces the reactivity by 0.096 Δk_{eff} for the 5 wt % case and 0.073 Δk_{eff} for the 8 wt % case. The overall impact of including the IFBA rods in the assembly cluster results is that 64 IFBA rods is sufficient to show that two 5 wt % assemblies in close contact would be subcritical; however, the higher enrichment assemblies would still be critical in this configuration. Sixty-four IFBA rods are still a relatively light load, and higher numbers of IFBA rods would be expected in these assemblies.

4. CONCLUSIONS

This report examines the impact of the LEU+ enrichments ranging up to 8.0 wt % and ATF concepts on fresh fuel storage areas at LWR nuclear plants. SCALE 6.2.4 CSAS calculations using the 252-group ENDF/B-VII.1 cross section library were performed to calculate best-estimate k_{eff} values for four representative classes of fuel storage systems: a PWR NFV, a BWR NFV, a low-density PWR SFP with intact absorber panels, and a low density PWR SFP with degraded absorbers. Each model had a baseline LEU enrichment of ~5 wt % UO_2. The enrichment of each model was increased to reflect potential LEU+ enrichment levels of 6.5 and 8.0 wt %. The effects of LEU+ fuel, as well as the ATF concepts Cr-coating, Cr-doping, and FeCrAl were analyzed relative to the baseline configurations in current operational analyses. For each configuration, the LEU+ and ATF calculations were used to calculate the changes from the baseline k_{eff} and maximum k_{eff} values by adding a representative sum of biases and uncertainties so that the result could be compared with the appropriate regulator limits. For cases in which the resultant maximum k_{eff} values exceed these limits, the use of integral burnable absorber credit and storage reduction were investigated to determine representative requirements. Although reactivity increases in LEU+ are expected, the potential for enrichment-dependent effects is of substantial interest.

The following effects were generally observed.

- Current PWR NFV configurations do not have sufficient margin to support LEU+ enrichments when fully flooded and have a reactivity impact of ~0.035 Δk_{eff} at 6.5 wt % fuel and ~0.06 Δk_{eff} at 8 wt %. Reasonable integral absorber credit successfully maintained compliance with regulatory limits.

- Current BWR NFV configurations do not have sufficient margin to support LEU+ enrichments when fully flooded. The sensitivity of BWR NFV resulted in supercritical configurations at all LEU+ enrichments and ATF concepts and have a reactivity impact of Δk_{eff} of ~0.08 at 6.5 wt % fuel and 0.12 at 8 wt %. Reduced assembly loading and/or increased absorber crediting was sufficient for regulatory limits. Whether this degree of LEU+ reactivity increase applies to BWR storage in general will be addressed in the next phase of the analysis, addressing BWR SFPs.

- Both examined low-density SFP configurations had sufficient margin to support LEU+ and had a reactivity impact of ~0.04 Δk_{eff} at 6.5 wt % fuel and ~0.065 Δk_{eff} at 8 wt %. Although the 8 wt % DA case was specifically supercritical, the margin of excess reactivity was ~25% the sum of biases and uncertainties overhead provided in this study. A more quantitative approach to bias could result in an acceptable margin.

- Cr-coated Zr claddings resulted in neutronic penalties of 0.003–0.005 Δk_{eff} in all storage models.

- Chromia-doped UO_2 had negligible neutronic impact.

- FeCrAl exhibited an enrichment-dependent heavy neutronic penalty. The penalty is ~0.03 Δk_{eff} in PWRs and ~0.02 Δk_{eff} in BWRs at nominal enrichments. PWRs show a higher enrichment-dependent penalty with the penalty decreasing in magnitude by ~0.008 Δk_{eff} at 8 wt % fuel, and the BWR penalty decreases by ~0.004 Δk_{eff} at 8 wt %, despite a lower nominal enrichment.

- Decoupling assumptions based around the 12 in. (30.48 cm) convention are true for LEU+ to the same extent as LEU.

- BWR eccentric positioning shows an enrichment-dependent increase in reactivity.

- Averaging of radial enrichment distributions, which is common in BWRs, has reduced conservatism with increasing enrichment.

- HALEU enrichments beyond LEU+ and approaching 20 wt % will require burnable absorber crediting or soluble boron content beyond practicality, as the enrichment increase from ~5 to 8 wt % strain regulatory limits while crediting non-negligible burnable absorber. The upper limit of ~20 wt % introduces a four times greater fissile inventory increase than that investigated in this study.

The next phase of this work will investigate high-density storage configurations, accounting for burned fuel for PWRs and maximum fuel reactivity of BWRs. How these enrichment-dependent effects perform as an additional function of burnup will be studied, as well as whether enrichment-dependent effects appear in instances in which they did not appear with fresh fuel.

5. REFERENCES

1. W. A. Wieselquist, R. A. Lefebvre, and M. A. Jessee, Eds., SCALE Code System, ORNL/TM-2005/39, Version 6.2.4, Oak Ridge National Laboratory, Oak Ridge, TN (2020).
2. 10 CFR Part 50.68. 2004. "Criticality Accident Requirements." *Code of Federal Regulations*, Title 10, *Energy*, Part 50, "Domestic Licensing of Production and Utilization Facilities."
3. *Susquehanna SES Unit 1 Cycle 4 Reload Summary Report*. 1987. Pennsylvania Power and Light Company. ADAMS Accession Number ML17146A850.
4. *Quad Cities Nuclear Power Station Updated Final Safety Analysis Report*. 2015. Chapter 9, "Auxiliary Systems." Rev. 13. ADAMS Accession Number ML19319A934.
5. *River Bend Station Unit 1, Application for License for Storage of Unirradiated Nuclear Fuel*. 1984. Gulf States Utilities Company. ADAMS Accession Number ML20084D030.
6. *Browns Ferry Nuclear Plant, Units 1, 2, and 3 - Application to Modify Technical Specification 4.3.1.2, Fuel Storage Criticality (TS-508)*. 2016. Tennessee Valley Authority. Adams Accession Number ML16225A663.
7. *License Amendment Request for Fuel Storage Changes*. 2012. Xcel Energy. ADAMS Accession Number ML12307A433.
8. *Clinton, Unit 1, Update Safety Analysis Report*. 2009. Chapter 9, "Auxiliary Systems." Rev. 16. ADAMS Accession Number ML14015A253.
9. O, Ozer et al. 2001. *Optimum Cycle Length and Discharge Burnup for Nuclear Fuel Phase 1: Results Achievable Within the 5% Enrichment Limit*. EPRI Report 1003133.
10. O. C. Brown et al. 2007. *Brunswick Nuclear Plant New Fuel Storage Vault Criticality Safety Analysis for ATRIUM™-10 Fuel*. AREVA Report ANP-2661 (NP), Revision 0.
11. R. Hall et al. 2021. *Extended-Enrichment Accident-Tolerant LWR Fuel Isotopic and Lattice Parameter Trends*. ORNL/TM-2021/1961. Oak Ridge: Oak Ridge National Laboratory.
12. *Guidance for Performing Criticality Analyses of Fuel Storage at Light Water Reactor Power Plants*. 2019. NEI-12-16, Rev. 4. Nuclear Energy Institute.
13. M. L. Fensin. 2004. *Optimum Boiling Water Reactor Fuel Design Strategies to Enhance Reactor Shutdown by the Standby Liquid Control System*, Master of Engineering Thesis, University of Florida.
14. R. M. Cumberland et al. 2021. *Isotopic and Fuel Lattice Parameter Trends in Extended Enrichment and Higher Burnup LWR Fuel Volume II: BWR Fuel*. ORNL/TM-2020/1835. Oak Ridge: Oak Ridge National Laboratory